eNeuro

Research Article: New Research | Development

The IgCAM BT-IgSF (IgSF11) is essential for connexin43-mediated astrocyte-astrocyte coupling in mice

https://doi.org/10.1523/ENEURO.0283-23.2024

Received: 6 July 2023
Revised: 19 January 2024
Accepted: 24 January 2024

1. **Manuscript Title: The IgCAM BT-IgSF (IgSF11) is essential for connexin43-mediated astrocyte-astrocyte coupling in mice**

2. **Abbreviated Title:** BT-IgSF controls astrocyte-astrocyte coupling

3. **List all Author Names and Affiliations:**

Laura Pelz[1], Laura Dossou[1], Nine Kompier[1], René Jüttner[1], Gabrielle Siemonsmeier[1], Niklas Meyer[1], Elijah D. Lowenstein[1], Ines Lahmann[1], Helmut Kettenmann[1,2], Carmen Birchmeier[1,3], and Fritz G. Rathjen[1]

1) Max-Delbrück-Center for Molecular Medicine, Robert-Rössle-Str. 10, DE-13092 Berlin, Germany
2) Shenzhen Institute of Advanced Technology, Chinese Academy of Sciences Shenzhen, China
3) NeuroCure Cluster of Excellence, Charité Universitätsmedizin Berlin, Corporate Member of Freie Universität Berlin and Humboldt-Universität zu Berlin, Berlin, Germany

4. **Author Contributions:** LP, LD, NK, GS, NM, EL, IL, RJ and FGR performed experiments, RJ, HK, CB and FGR evaluated data. FGR drafted and wrote the final version of the manuscript.

5. **Correspondence should be addressed to**

Fritz G. Rathjen, Max-Delbrück-Center, Robert-Rössle-Str. 10, DE-13092 Berlin, Germany, (rathjen@mdc-berlin.de)

6. **Number of Figures: 7, extended Figures 4**
7. **Number of Tables: 1**
8. **Number of Multimedia: 0**
9. **Number of words for Abstract: 187**
10. **Number of words for Significance Statement: 70**
11. **Number of words for Introduction: 783**
12. **Number of words for Discussion: 1843**

13. **Acknowledgements**

We thank Mechthild Henning for technical assistance and Karola Bach, Stefanie Rode and Petra Stallerow for mouse breeding. We thank Dr. Thomas Müller (MDC) with the help in assembling Figure 4. We thank Dr Christopher Patzke (University of Notre Dame, USA) for the critical reading of the manuscript. FGR is an emeritus professor at the MDC. We acknowledge the advice of Dr. Frank Konietschke (Institut für Biometrie und Klinische Epidemiologie Charité, Berlin, Germany) on the statistical evaluations of our data.

Present addresses: Laura Pelz: National Center for Tumor Diseases (NCT) Heidelberg and the German Cancer Research Center (DKFZ), Im Neuenheimer Feld 460, 69120 Heidelberg, Germany.
Laura Dossou: Pfizer Pharma GmbH, Linkstraße 10, 10785 Berlin, Germany
Gabrielle Siemonsmeier: McGill University, Integrated Program in Neuroscience, Irving Ludmer Building, 1033 Pine Avenue West, Montréal, Québec H3A 1A1, Canada
Niklas Meyer: Department of Neurology with Institute of Translational Neurology, University of Münster, DE-48149 Münster, Germany.
Elijah D. Lowenstein: Department of Medicine, Division of Endocrinology, Diabetes and Metabolism. Beth Israel Deaconess Medical Center and Harvard Medical School, Boston, MA 02115, USA.

14. **Conflict of Interest**

Authors report no conflict of interest

Funding sources This work was supported in part by funds from the Deutsche Forschungsgemeinschaft SFB 665 to FGR, KE329/28 to HK, GO865/13-1 to Dr Michael Gotthardt (MDC), EXC-2049 – 39068808 (Germany's Excellence Strategy) to CB and the MDC.

The IgCAM BT-IgSF (IgSF11) is essential for connexin43-mediated astrocyte-astrocyte coupling in mice.

Abstract

The type I transmembrane protein BT-IgSF is predominantly localized in the brain and testes. It belongs to the CAR subgroup of Ig cell adhesion proteins, that are hypothesized to regulate connexin expression or localization. Here, we studied the putative link between BT-IgSF and connexins in astrocytes, ependymal cells and neurons of the mouse. Global knockout of BT-IgSF caused an increase in the clustering of connexin43 (Gja1), but not of connexin30 (Gjb6), on astrocytes and ependymal cells. Additionally, knockout animals displayed reduced expression levels of connexin43 protein in the cortex and hippocampus. Importantly, analysis of biocytin spread in hippocampal or cortical slices from mature mice of either sex revealed a decrease in astrocytic cell-cell coupling in the absence of BT-IgSF. Blocking either protein biosynthesis or proteolysis showed that the lysosomal pathway increased connexin43 degradation in astrocytes. Localization of connexin43 in subcellular compartments was not impaired in astrocytes of BT-IgSF mutants. In contrast to connexin43 the localization and expression of connexin36 (Gjd2) on neurons was not affected by the absence of BT-IgSF. Overall, our data indicate that the IgCAM BT-IgSF is essential for correct gap junction-mediated astrocyte-to-astrocyte cell communication.

Significance Statement

Astrocytes regulate a variety of physiological processes in the developing and adult brain that are essential for proper brain function. Astrocytes form extensive networks in the brain and communicate via gap junctions. Disruptions of gap junction coupling are found in several diseases such as neurodegeneration or epilepsy. Here, we demonstrate that the cell adhesion protein BT-IgSF is essential for gap junction mediated coupling between astrocytes in the cortex and hippocampus.

Key words: IgCAM, BT-IgSF, gap junctions, connexin43, astrocyte-astrocyte coupling

Introduction

BT-IgSF (brain- and testis-specific Ig superfamily protein, also known as IgSF11) is a cell adhesion protein belonging to a small subgroup of IgCAMs consisting of CAR (coxsackievirus and adenovirus receptor), ESAM (endothelial cell-selective adhesion molecule) and CLMP (CAR-like membrane protein). The group shares a similar overall domain organization with an N-terminal V-type and a C2-type Ig domain and a highly related amino acid sequence (Owczarek et al., 2023; Raschperger et al., 2004; Rathjen, 2020; Xie et al., 2021). Initially BT-IgSF was described as a novel IgSF member that was preferentially expressed in the brain and testis (Suzu et al., 2002). Independently of this report BT-IgSF was also found to be up-regulated in intestinal-type gastric cancers and termed IgSF11 (Katoh and Katoh, 2003). Moreover, it was also termed V-set and Immunoglobulin domain containing 3, abbreviated VSIG-3, due to its binding to VISTA (Wang et al., 2019). The BT-IgSF gene is located on chromosome 3 in humans and chromosome 16 in mice. The cytoplasmic segment of BT-IgSF contains a PDZ-binding motif at its C-terminus that interacts with the scaffolding protein PSD95 (Jang et al., 2015). Adhesion assays with heterologous cells showed that BT-IgSF promotes homotypic cell binding (Eom et al., 2012; Harada et al., 2005).

So far, the function of BT-IgSF (IgSF11) has been studied in neurons, Sertoli and germ cells of the testes, during osteoclast differentiation and in the organization of pigment cells in fish (Ahi and Sefc, 2017; Chen et al., 2021; Eom et al., 2012; Hayano et al., 2021; Jang et al., 2015; G. M. Kim et al., 2023; H. Kim et al., 2023; Kim et al., 2020; Pelz et al., 2017; Singh and Nusslein-Volhard, 2015). Knockdown studies using cultured mouse hippocampal neurons indicated that BT-IgSF is implicated in synaptic transmission through a tripartite interaction with PSD95 and AMPA receptors (Jang et al., 2015). Consequently, global BT-IgSF-deficient mice displayed a moderately decreased excitatory synaptic strength in the dentate gyrus and long-term potentiation in hippocampal CA1 neurons and behavioral deficits (Jang et al., 2015;

Montag et al., 2023). In another study analyzing neurons BT-IgSF (IgSF11) was found to regulate chandelier cell axon innervation of pyramidal neuron initial axon segments (Hayano et al., 2021).

In the murine testis BT-IgSF is expressed in Sertoli cells at the blood-testes barrier, a structure that opens and closes to allow the passage of germ cells. In a global knockout, the absence of BT-IgSF causes a malfunction of the blood-testes-barrier leading to male infertility due to the mislocalization of connexin43. Connexin43 was found throughout the seminiferous epithelium instead of being restricted to the blood-testes barrier as it is in wildtype animals. Therefore BT-IgSF might regulate the localization or activity of connexin43 in Sertoli cells (Pelz et al., 2017). In line with this finding connexin43 was found to play an essential role in tight junction reassembly at the blood-testes barrier during its restructuring processes (Li et al., 2010). A critical role of BT-IgSF in regulating the organization of pigment cells into stripes along the dorso-ventral or anterior-posterior body axes was observed in zebrafish and *Neolamprologus meeli* (Ahi and Sefc, 2017; Eom et al., 2012; Singh and Nusslein-Volhard, 2015). Similar irregular patterns of chromatophores were described in zebrafish with mutations in connexin 41.8 and connexin39.4, suggesting a functional link between BT-IgSF and connexins. This link might also be anticipated from the mislocalization of connexin43 in Sertoli cells of BT-IgSF knockout mice (Haffter et al., 1996; Irion et al., 2014; Pelz et al., 2017; Watanabe et al., 2006; Watanabe and Kondo, 2012). Together, these data suggest an essential function of BT-IgSF in regulating the localization or activity of connexins as shown for other members of the CAR subgroup.

To further investigate the functional interaction between BT-IgSF and connexin43, we investigated its role in the brain on glial cells. Here, we show that BT-IgSF is strongly localized on the surface of astrocytes and ependymal cells in addition to its previously described neuronal expression (Higashine et al., 2018; Jang et al., 2015; Suzu et al., 2002). In the absence of BT-IgSF in a global mouse knockout we observed that the localization of connexin43 on astrocytes

and ependymal cells was aberrantly clustered. Additionally, we uncovered a severe reduction in connexin43 on astrocytes at the protein level. Consequently, dye-loading experiments revealed reduced diffusion within the astrocytic network in the hippocampus as well as in the cortex of mutant mice. We discuss these findings in the context of the function of the related proteins CLMP and CAR which also affect the expression and localization of connexin43 and 45 in smooth muscle cells of the intestine and in cardiomyocytes, respectively (Langhorst et al., 2018; Lim et al., 2008; Lisewski et al., 2008; Matthaeus et al., 2023; Rathjen, 2020).

Material and Methods

Mice

The global knockout of BT-IgSF (B6-Igsf11$^{tm1e(KOMP)Wtsi}$/FGR) and its genotyping has been described elsewhere (Pelz et al., 2017). Breeding was either from tg/wt to tg/wt or tg/tg (female) to wt/tg (male). Heterozygous BT-IgSF mice did not differ from wt/wt mice (Pelz et al., 2017). Cx36-deficient mice (B6.129P2-Gjd2tm1Kwi/Cnrm; EM:00326) were obtained from the European Mouse Mutant Archive (EMMA) and genotyped as described (Güldenagel et al., 2001). Animals were housed on a 12/12 h light/dark cycle with free access to food and water. The animal procedures were performed according to the guidelines from directive 2010/63/EU of the European Parliament on the protection of animals used for scientific purposes. All experiments were approved by the local authorities (LaGeSO) (numbers T0313/97, X 9007/16, X9008/20, O 0038/08 and H0027/20). Wildtype littermates served as controls.

Cell culture, antibodies and immunocytochemistry

Hippocampal cells were prepared from postnatal day 2 or 3 mice and cultured on poly-D-lysine coated coverslips in 24-well plates at a density of 7.5 x 10^4 cells/ml in Neurobasal (Invitrogen) supplemented with B27 (Invitrogen) and 10% FCS (Gibco) for 10 days. Every third day half of the culture medium was removed and replaced by Neurobasal/B27 without FCS. Glial cells from postnatal day 2/3 cortices or hippocampi were prepared according to standard procedures and were maintained in DMEM supplemented with 10% FCS and penicillin/streptomycin in 75 cm^2 flasks until confluent (McCarthy and de Vellis, 1980). Then, astrocytes were detached by trypsin/EDTA treatment and further grown in multiple 24 well cluster (200 000 cells per well) for cycloheximide or chloroquine treatment (see below) or on

poly-D-lysine coated coverslips (20 000 cells per 12 mm diameter coverslip) for staining with antibodies to specific intracellular compartments (see below). Cells of each 24 well cluster were extracted as described below and equal amounts were analyzed by Western blotting (see below). For immunocytochemistry cells were fixed in 4% paraformaldehyde/PBS for 10 minutes, washed with PBS/1% BSA. For staining of cryosections (thickness 12-16 µm) by indirect immunofluorescence, adult mice were transcardially perfused with 50 ml PBS followed by 50 ml 4% paraformaldehyde. Brains were post fixed for 5 hours and then transferred into 15% followed by 30% (w/v) sucrose in PBS to obtain cryoprotection. Primary and fluorophore-conjugated secondary antibodies were applied in blocking solution (5% goat serum, 1% BSA, 0.1% Triton X-100 in PBS). Mouse monoclonal antibodies were incubated on sections using the MOM immunodetection kit from Vector Laboratories (BMK-2202). Sections or monolayer cultures were counterstained with the nuclear stain DAPI at 1 µg/ml. For antibodies see table 1.

Microscopic images were obtained at room temperature by confocal imaging using a Carl Zeiss LSM 700 Laser Scanning Microscope equipped with ZEN 2011 software and the following lenses: a Plan-Neofluar 20x/0.30 NA objective, a Plan-Achromat 40x/1.3 Oil, a Plan-Achromat 63x/1.40 NA oil objective or a Plan Apochrome 100x/1.40 oil objective (all from Carl Zeiss MicroImaging, GmbH). Figures were assembled using Illustrator CS5 (Adobe).

To quantify connexin43 clusters confocal images were taken with a 63x objective from cryosections and a 100x objective for cultured astrocytes. Quantification of connexin43 clusters was done by Fiji software setting threshold to RenyiEntropy routine; clusters were accepted between 0.05 and 1.00 μm^2 (2-40 pixels). Primary branches of astrocytes and the density of astrocytes were counted from hippocampal slices stained by anti-GFAP and DAPI positive cells.

Analysis of localizations or co-localizations of connexin43 to intracellular compartments were done with antibodies to γ-adaptin, LAMP-1, ZO-1, GM130, to phalloidin-Alexa594 (6.6 µM;

1:500; Thermo Scientific #A12381) or to BT-IgSF (Rb96) (see table 1) on 4% paraformaldehyde/PBS-fixed (5 minutes on ice) on wildtype and knockout astrocyte cultures. Assessment of cell surface localization of connexin43 cluster on knockout astrocytes was done by life staining of astrocytes with WGA-488 (1 µg/ml; ThermoFisher Scientific W11261) at 4^0 C for 45 minutes followed by washing, PFA fixation and solubilization with 0.1% Triton-X100. Then rabbit antibodies to connexin43 were added as described above. Images were obtained by confocal microscopy using the 100x oil objective mentioned above and were analyzed using Fiji/Image J. Calculation of the Pearson correlation was determined by Coloc 2 derived intensity-based correlation analysis from regions of interest around connexin43 clusters (10 µm circles). Costes threshold regression was applied and Pearson´s R value (P) above threshold was used, data were accepted with an Costes p-value >0.95. Mann-Whitney U-test (GraphPad Prism 6.07) was used to compare wildtype with knockout values.

Generation of a connexin 36 fusion protein and polyclonal antibodies to connexin36.

Since several commercial anti-connexin36 antibodies were of limited use in our hands we generated polyclonal anti-mouse connexin36 antibodies in rabbits using a fusion protein that comprised the second cytoplasmic segment of mouse connexin36 (amino acid residues 99 – 197) attached to a histidine stretch. The cDNA of this segment was synthesized by Invitrogen and cloned into plasmid pMA-RQ and further subcloned into the bacterial expression vector pET-14b (Novagen/EMD Millipore). The protein was expressed in Bl21 bacteria with the addition of IPTG to a final concentration of 1 mM. Bacteria were harvested by centrifugation and frozen at -80^{o}C. Bacterial pellets were resuspended in ice-cold lysis buffer containing 2 M Urea, 50 mM Tris, 150 mM NaCl, pH 7.4, supplemented with protease blockers (aprotinin, PMSF, leupeptin, pepstatin). Unsolubilized material was removed by centrifugation and the supernatant was precipitated by ammonium sulfate (50% saturation). The pellet was dialyzed against 10 mM Tris, pH 11 and run over an anion exchange column (DE52 Whatman). The

unbound fraction was applied to an NTA column (Qiagen), washed with PBS followed by 20 mM imidazole and bound protein was eluted by 200mM imidazole. Purity was analyzed by 15% SDS PAGE. Rabbits were injected with 100 µg protein in Freund's adjuvant at fortnightly intervals. The IgG fraction was obtained by protein A affinity chromatography (GE Health Care) and further purified by affinity chromatography on an affinity column containing the above mentioned connexin36 segment protein coupled to CNBr-activated Sepharose (14 mg to 2.5 g Sepharose 4B; GE Healthcare). The specificity of the affinity purified antibodies was tested on tissue extracts and cryostat sections (12 µm thick, mildly fixed with 1% paraformaldehyde/PBS for 1 minute on ice) from wildtype or connexin36-deficient mice (see Figure 7).

Biochemical methods

To obtain a crude membrane fraction from tissues of BT-IgSF knockout or wildtype mice of different ages (as indicated in the Figure legends), hippocampi or cortices were homogenized in 0.34 M sucrose supplemented with protease blockers [aprotinin (20 U/µl), leupeptin (5 mM), pepstatin (5mM), PMSF (1mM)]. Nuclei were pelleted at 200xg for 10 minutes and the resulting supernatant was centrifuged at 100 000xg for 10 minutes to obtain a crude membrane pellet and cytoplasmic fraction in the supernatant. Membranes were stripped with 0.1 M diethylamine (pH11.5), supplemented with protease blockers to remove peripheral membrane proteins. The membrane fraction was first solubilized in 1% Triton-X100 and un-solubilized material was removed by centrifugation. The pellet was then solved in 1% SDS in PBS supplemented with protease blockers and un-solubilized material was again removed by centrifugation (Musil and Goodenough, 1991). Protein concentrations were determined using the Bradford assay (Bio-Rad #500-0006) and spectrophotometric measurements. Equal amounts of proteins were loaded on SDS-PAGE for Western blotting which was controlled by Ponceau protein stain and housekeeping proteins such as GAPDH, heavy chain of clathrin, or

α-tubulin. Depending on the tissue or antibody, 10, 15 or 20 µg of protein was loaded per lane. Blots to identify BT-IgSF in cells or tissues SDS-PAGE was run without reducing agents. For the calculation of the molecular mass of connexin36 in neural tissues the following molecular mass standards were used (in kDa): Conalbumin, 76; BSA, 66¸actin, 43; GAPDH, 36 and carbonic anhydrase, 31.

Cycloheximide chase experiments (100 µg/ml, Sigma, C-7698, dissolved in DMSO and diluted 1:500 in the incubation medium) were done with wildtype and BT-IgSF knockout astrocytes cultures for times indicated in the Figure 3G to H. 200 000 cells were grown in 24 well clusters in DMEM/10% FCS and washed two times with DMEM without FCS before the addition of cycloheximide. Chloroquine experiments (100 µM; Sigma C6628, dissolved in PBS) to inhibit lysosomal degradation were done with wildtype and BT-IgSF knockout astrocytes cultures for 4 hours in DMEM without FCS (Schrezenmeier and Dörner, 2020; Wu et al., 2016). Treatment of wildtype astrocytes with tumor necrosis factor-α (1 ng/ml; Sigma T5944) or interferon-γ (10 ng/ml; Sigma I17001) were done in DMEM without FCS for 24 hours. In these blocking experiments cells were lysed in TBS (pH 7.4) with 1% SDS and 1 mM EDTA supplemented with protease blockers and boiled in SDS-PAGE sample buffer. Equal amounts of protein were loaded on 10% SDS PAGE, blotted and analyzed with rabbit anti-connexin43 or rabbit 96 to BT-IgSF. Equal loading was controlled by Ponceau protein stain and mAb to GAPDH. Quantification of connexin43 bands was done using Image Lab software (BioRad) and analyzed by Mann-Whitney-test and Two-Way ANOVA (GraphPad Prism 6.07). Total connexin43 expression was derived from the sum of connexin43 bands P0, P1 and P2 (bands P1 and P2 correspond to phosphorylated connexin43).

RNAscope on hippocampus sections

In situ fluorescent hybridization was performed using the RNAscope Multiplex Fluorescent Assay from ACDbio according to the manufacturer's instructions (Wang et al.,

2012). Briefly, PFA-fixed hippocampus or midbrain sections of 20 µm thickness were obtained from P20 or P10 wildtype mice, respectively, and stored at -80°C until use. Sections were thawed at 37°C for 10 minutes and post-fixed in 4% PFA in PBS for 15 minutes before washing in PBS and continuing with the manufacturer's instructions. Protease treatment was performed using Protease IV. RNAscope probes against BT-IgSF (C1 - 451131), GFAP (C2 - 313211), vGlut1 (C2 - 416631) and GAD65/67 (Gad1: C2 – 400951; Gad2: C2 – 439371 were used.

Dye coupling in acute brain slices

To characterize the tracer spread within coupled astrocytic networks acute brain slices containing the hippocampus or the cortex were prepared from 8–10-week-old knockout or littermate controls of either sex as described previously (Maglione et al., 2010). In brief, mice were sacrificed by cervical dislocation, decapitated and their brains carefully removed and mounted in a chamber with ice-cold bicarbonate-buffered artificial cerebrospinal fluid (ACSF), composed of (in mM): NaCl 134; KCl 2.5; $MgCl_2$ 1.3; $CaCl_2$ 2; K_2HPO_4 1.25; $NaHCO_3$ 26; D-glucose 10; pH 7.4. The buffer solution was continuously gassed with carbogen (95% O_2, 5% CO_2). Coronal slices of 250 µm were prepared at 4°C using a vibratome (HM 650 V, Microm International GmbH, Walldorf, Germany), and stored in ACSF at room temperature (21–25°C) for up to 5 hours.

Before dye filling, slices were incubated for 20 minutes in 1µM sulforhodamine 101 (SR-101) at 35°C to label astrocytes. Astrocytes were identified by their SR-101 fluorescence at excitation and emission wavelengths of 555 and 585 ± 10 nm, respectively, using a 60x water-immersion objective (Olympus, Hamburg, Germany). For recording and for dye loading, a patch pipette (pulled from borosilicate glass, 1.5 mm outside diameter, 0.315 mm wall thickness) was filled with a solution containing 30 mM KCl, 1 mM $MgCl_2$, 0.5 mM $CaCl_2$, 100 mM potassium-gluconate, 10 mM Hepes, 5 mM EGTA, 0.5% biocytin (Sigma-Aldrich) and 3 mM Na_2ATP, pH 7.3. Lucifer Yellow (10 µg/ml; Sigma-Aldrich) was added to the pipette

296 solution and intracellular access of the solution was confirmed by excitation at 495 nm and
297 visualization at an emission wavelength of 510 ± 10 nm. The pipette resistance ranged from 5
298 – 8 MΩ. Cells were passively dialyzed via the patch pipette for 20 min. In order to confirm cell
299 identity and vitality, membrane currents were recorded with a series of de- and hyperpolarizing
300 voltage steps (10 mV each, filtered at 2.9 kHz) from a holding potential of -70 mV ranging
301 from -160 to +50 mV for 50 ms), using an EPC 10 patch-clamp amplifier and TIDA 5.25
302 software (HEKA Elektronik, Lambrecht, Germany), as described previously (Richter et al.,
303 2014). Capacitive transients from the pipette were compensated online via the patch clamp
304 amplifier (C_{fast}) whereas membrane capacity and series resistance (C_{slow}) were not compensated.
305 The calculated liquid junction potential of the used intra cellular solutions was – 8.858 mV
306 using Patchers Power Tools (Mendez & Würriehausen, Göttingen, Germany) and Igor Pro 7
307 software (Wavemetrics, Portland, OR, USA). The calculated reversal potentials of astrocytes
308 were corrected for the liquid junction potential. Only cells whose series resistance was not
309 higher than 125 % at the end of the dialysis phase compared to the beginning of the recording
310 were taken into account for the following immunohistochemical experiments and the
311 calculation of the membrane properties. After dye loading and patch-clamp recording, the
312 pipette was carefully removed from the cell in order to disrupt the patch.

313 Slices were subsequently fixed in a solution of 4% paraformaldehyde in 0.1 M
314 phosphate buffered saline (pH 7.4) overnight at 4°C. After fixation, slices were incubated in a
315 solution containing 2% Triton-X100, 2% BSA and 5% normal donkey serum in Tris-buffered
316 saline at pH 7.4 for 2 h at room temperature to permeabilize and to block nonspecific binding
317 of the primary antibodies. Biocytin-filled networks were visualized with Cy3-conjugated
318 streptavidin (1:200; Jackson ImmunoResearch, Hamburg, Germany). In addition, rabbit anti-
319 BT-IgSF (Rb95) and guinea pig anti-GFAP antibodies were applied to label BT-IgSF and
320 astrocytes, respectively. The floating slices were incubated with primary antibodies for 48 h at
321 4°C followed by secondary antibodies and DAPI. For additional antibodies see table 1.

Slices were rinsed and mounted with Aqua Poly/Mount (Polysciences Inc., Washington, USA). Images were acquired by a Leica DM TCS SPE confocal microscope (HC APO 20x/0.75; Leica, Solms, Germany) with Leica software (LCS Lite or LAS AF Lite, respectively). Step size between z-planes in the confocal stacks was about 1 µm, but the number of imaged planes in each stack varied from slice to slice. Images were analyzed by Fiji/Image J software, using the cell counter plugin and z-axis projection functions.

Statistics

Significance of data were tested using nested t-test, Mann-Whitney-test, unpaired t-test with Welch correction or One-Way ANOVA using GraphPad Prism software (version 6.07 and version 10.1.2) after excluding outlier using the outlier tests (ROUT, Q=1%). Normality was tested using the D'Agostino & Pearson omnibus normality test or Shapiro-Wilk normality test.

Results

Absence of BT-IgSF disrupts the expression and localization of connexin43 in the hippocampus and on cultured astrocytes

BT-IgSF was first described as an IgSF member that was preferentially expressed in the brain and testis (Suzu et al., 2002). BT-IgSF and related proteins of the CAR family of adhesion proteins have been proposed to modulate the localization of connexins (Rathjen, 2020). We tested whether the absence of BT-IgSF affects the localization of connexin43 expression on astrocytes as it does on Sertoli cells in the testes (Pelz et al., 2017). In the mature brain connexin43 is expressed by astrocytes and ependymal cells, but not by neurons. Connexin30 and connexin26 have also been detected in adult astrocytes, albeit at lower levels (Dermietzel et al., 1989; Nagy et al., 2004). Hippocampal sections as well as astrocyte monolayer cultures were labeled with rabbit anti-connexin43 antibodies. Microscopic images of hippocampal sections revealed an altered localization of connexin43 in BT-IgSF knockout tissue (Figure 1A and B). In the molecular layer of knockout hippocampal tissue, a pronounced decrease in the number of cennexin43 spots (31% of the wildtype), accompanied by a marked increase in the connexin43 spot size (average of 0.19 to 0.5 μm^2 in wildtype and BT-IgSF-/- mice, respectively) was observed in high power magnifications (Figure 1C, E and F). Similar observations on the clustering and number of connexin43 spots were made on cultured astrocytes, suggesting that BT-IgSF might control connexin43 localization even in the absence of neurons (Figure 1D, H and I). Analysis of the distribution of the number of counts versus cluster size further highlights the difference between wildtype and BT-IgSF knockouts (Figure 1G and J). Taken together, our data indicate that the absence of BT-IgSF decreases the number of connexin43 spots but increases their clustering in astrocytes.

We further investigated BT-IgSF expression on neural cells by immunocytochemistry of hippocampal cultures and brain sections. In monolayer cultures prepared from newborn

hippocampal tissue BT-IgSF was primarily localized on the surface of GFAP-positive astrocytes (Figure 2A and B and Extended Figure 2-1 on the specificity of the anti-BT-IgSF antibody) and was not or only weakly detected on MAP2-positive dendrites (Figure 2C). However, single molecule fluorescent *in situ* hybridization (RNAscope) experiments indicated that neurons express detectable amounts of *Bt-igsf* mRNA (Extended Figure 2-2). Similarly, *Bt-igsf* mRNA was found in GFAP–positive cells in sections of the molecular layer of the hippocampus (Figure 2E and F), which is further supported by immunohistochemistry using polyclonal antibodies to the extracellular region of BT-IgSF (Figure 2D). BT-IgSF protein expression increases as the brain matures postnatally and effective solubilization from crude membrane fractions requires ionic detergents such as SDS (Figure 2G - J).

To analyze connexin43 in Western blots, hippocampus and cortex crude membrane fractions from wildtypes and mutants were prepared. Membranes were first treated by Triton-X100 containing buffer followed by SDS of the pellet to separate soluble (primarily non-junctional) from insoluble (mainly junctional) connexin43. Significant decreases in connexin43 levels in both Triton-X100- and SDS-containing fractions were found in the mutant (Figure 3A and B). In contrast to connexin43, connexin30, which is also implicated in the extensive network organization of astrocytes and which can also form gap junction channels together with connexin43 (Nagy et al., 2004; Willecke et al., 2002), is not reduced nor is its overall localization changed in the hippocampus in the absence of BT-IgSF (Figure 3C and D). No changes in GFAP protein level were detected (Figure 3E and F) in the hippocampus of BT-IgSF mutants. This indicated that the reduction in connexin43 levels was not caused by a decrease in GFAP i.e., a decrease in the number of astrocytes (see also Figure 5K to N).

Connexin43 has a high turnover rate. Therefore, the reduced expression of connexin43 might be caused by decreased biosynthesis, increased degradation by multiple pathways or by trafficking deficits from the cytoplasm to the plasma membrane (Falk et al., 2016; Laird and Lampe, 2018). We measured connexin43 protein levels using Western blots in a chase

experiment after adding the protein synthesis blocker cycloheximide in wildtype and BT-IgSF knockout astrocyte cultures. In both cultures, the amount of connexin43 protein significantly decreased in the presence of cycloheximide. After 180 minutes of incubation with cycloheximide the level of connexin43 protein decreased to 60 percent of baseline in both genotypes (Figure 3G and H). However, no differences between wildtype and knockout cultures were detected at different incubation periods. Linear regression analysis revealed that 50% of connexin43 would be present after 210.0 minutes and 235.1 minutes in wildtype and knockout astrocytes, respectively ($p=0.8869$, unpaired t-test with Welch's correction). Interestingly, the addition of the lysosome inhibitor chloroquine for 4 hours led to an increase in connexin43 protein in knockout cultures (to 126% on average) but only sparely in control cultures (105%) (Figure 3I and J) as the change in the latter did not reach statistically significance. These data might indicate that degradation of connexin43 is increased in BT-IgSF knockout cultures and suggest that BT-IgSF contributes to the stabilization of connexin43. Furthermore, a change in the migration pattern of connexin43 in SDS-PAGE under chloroquine conditions was detected in astrocytes of both genotypes (Figure 3I). The connexin bands pattern became more diffuse, band P1 appeared weaker and all bands migrated at a slightly higher position - perhaps indicating increased phosphorylation. The latter shift was stronger in the control. In summary, in the absence of BT-IgSF degradation of connexin43 via the lysosome pathway is increased which might explain the reduced expression of connexin43 in the hippocampus and cortex of BT-IgSF-/-.

To test for subcellular localization defects of connexin43 in the absence of BT-IgSF we compared wildtype and BT-IgSF-deficient astrocytes by staining them with antibodies specific for different compartments including LAMP-1 (lysosomal-associated membrane protein 1), phalloidin (actin cytoskeleton), GM130 (cis-Golgi marker), γ-adaptin (secretory vesicles), and ZO-1 (sub compartments such as tight junctions at the cell surface). No increased co-localization between connexin43 and any of these subcellular markers was detected in mutants

indicated by a comparison of the Pearson correlation coefficients (Figure 4A to D). This might exclude that connexin43 gets retained in an intracellular compartment in BT-IgSF-/- astrocytes. Consequently, connexin43 clusters were found at the cell surface in close association with wheat germ agglutinin that was applied to living astrocyte cultures on ice (Figure 4E). Taken together these data do not support the notion that the absence of BT-IgSF reduces the expression of connexin43 in astrocytes via impaired intracellular trafficking.

We detected minimal co-localization between connexin43 and the tight junction protein ZO-1 (mean value of Pearson's R-value: 0.1631 for wildtype and 0.002 for knockout) that was further slightly decreased in the BT-IgSF knockout, possibly due to the fact that connexin43 was present at reduced levels (Figure 4F). In addition, BT-IgSF itself showed very little co-localization with connexin43 (Figure 4G). The occasional co-localization observed could be due to the fact that all of these proteins are present at the plasma membrane, or might indicate weak and/or transient associations (mean value of Pearson's R-value: -0.004568). A direct association between BT-IgSF and connexin43 could not be demonstrated since the available antibodies failed to co-precipitate BT-IgSF and connexin43.

Previously published studies reported that both the tumor necrosis factor-α and interferon-γ reduce the expression of connexin43 on astrocytes and enterocytes, which in turn impairs cell-cell communication (Hinkerohe et al., 2005; Leaphart et al., 2007; Meme et al., 2006; Zhang et al., 2015, 2013). Conversely, BT-IgSF (VSIG3) was found to inhibit the secretion of interferon-γ and tumor necrosis factor-α of activated PBMCs and CD4-positive T-cells in cell culture assays (Xie et al., 2021).Therefore, we applied interferon-γ and tumor necrosis factor-α to wildtype astrocyte cultures. Interestingly, BT-IgSF protein level was diminished in both treatments which might further strengthen our data on a functional link between BT-IgSF and connexin43 on astrocytes (Figure 4H and I). As expected connexin43 was also found to be reduced (Figure 4J).

Reduced astrocyte-astrocyte coupling in the hippocampus and cortex in the absence of BT-IgSF

A typical feature of astrocytes in the brain is their organization in vast networks that communicate with one another via gap-junction channels formed by connexins (Giaume et al., 2010). In order to investigate the effect of BT-IgSF ablation on astrocytic network size in the hippocampus and cortex we performed dye-coupling experiments (see schemes shown in Figure 5A to C). Astrocytes were identified in acutely isolated mouse brain slices by sulforhodamine 101 that specifically labels astroglia (Nimmerjahn et al., 2004). Individual astrocytes in the hippocampus molecular layer or cortical layers II – IV from horizontal slices were dye-loaded with biocytin via patch pipette. Diffusion of the dye throughout the astrocytic network allows for the visualization and quantification of the extent of gap-junction mediated cell-cell coupling (Figure 5D).

In the hippocampus as well as in the cortex, the number of coupled astrocytes per injected cell was significantly decreased in mutant animals. 15 dye-filled slices from 3 control mice and 11 slices from 4 BT-IgSF knockout mice were used for immunohistochemical analysis of hippocampal coupled astrocytic networks. On average 101±8.851 (mean ± SD) biocytin-positive hippocampal astrocytes were coupled in the wildtype, whereas in the knockout only 78±7.837 (mean ± SD) biocytin-positive astrocytes were found to form a network (Figure 4E to G). In the cortex the differences between wildtype and knockout were even more pronounced: on average 118±20.95 (mean ± SD) astrocytes in control and only 48±7.86 (mean ± SD) in the BT-IgSF knockout form a network (11 dye-filled slices from 4 controls and 10 slices from 4 knockouts) (Figure 5H to J). Extended Figure 5-1 illustrates the passive membrane properties of hippocampal astrocytes in both groups over the course of the dialysis period. We observed no significant differences in the current to voltage relationship, membrane resistance or membrane capacitance ($p>0.05$) between genotypes or between the start and the end of the

dialysis period, indicating that these factors were not responsible for the change in the extent of the astrocytic network. Similar results were obtained for passive membrane properties in cortical astrocytes. Further, neither the density of GFAP-positive astrocytes nor their complexity (arborization) was reduced in the absence of BT-IgSF, suggesting that altered morphological parameters of astrocytes are unlikely to cause reduced cell-cell coupling in the absence of BT-IgSF (Figure 5K to N).

In summary, we detected reduced astrocyte-astrocyte coupling in the hippocampus and the cortex in the absence of BT-IgSF. We assign this to the observed changes in connexin43 expression, i.e., the reduction of the connexin43 protein levels and/or its altered clustered localization.

Absence of BT-IgSF disrupts the localization of connexin43 on ependymal cells

Ependymal cells are specialized multi-ciliated glial cells that line the ventricles and form an interface between the cerebrospinal fluid (CSF) and brain parenchyma (Deng et al., 2023). These cells also express GFAP (Roessmann et al., 1980). Ependymal cells contact each other via connexin43 containing gap junctions and are implicated in barrier formation as well as the production and circulation of cerebrospinal fluid (Saunders et al., 2018). To ask whether the absence of BT-IgSF also affects the localization of connexin43 on ependymal cells, we characterized the expression of BT-IgSF in the brain by immunohistochemistry. We detected a strong localization of BT-IgSF on cells lining all brain ventricles at embryonic as well as postnatal stages, but only very weak staining in the neural tissue directly adjacent to the ependymal cell layer (Figure 6A, see also Extended Figure 6-1 for antibody specificity). Higher magnifications showed that BT-IgSF was found at the lateral and basal surfaces of ependymal cells, but not at the apical side that faces the ventricle (Figure 6B). The choroid plexus that expresses the related IgCAM CAR stained weakly for BT-IgSF (Figure 6C). Matching the

deficits that we found in astrocytes, we also found a decreased number of spots and an increased clustering of connexin43 in BT-IgSF mutant ependymal cells compared to wildtypes (Figure 6D to G).

The localization of connexin36 in neurons is not affected by the absence of BT-IgSF

In the brain, connexin43 is restricted to astrocytes, whereas connexin36 is the main connexin in neurons and is primarily expressed during embryonic and early postnatal developmental stages (Condorelli et al., 1998; Degen et al., 2004; Gulisano et al., 2000; Rubio and Nagy, 2015; Söhl et al., 1998). We therefore asked whether the absence of BT-IgSF also affects the localization of the gap junction protein connexin36 in neurons. Commercially available antibodies to connexin36 were of limited use in our hands, and we therefore generated a polyclonal antibody to the cytoplasmic stretch (residues 99 to 197) of mouse connexin36 (Figure 7A - D). Although this antibody also showed some unspecific binding in Western blots, it clearly labeled connexin36 at a molecular mass of 34 kDa in wildtype but not in connexin36-deficient neural tissues (Figure 7D). The specificity of this antibody to connexin36 could also be demonstrated in sections of wildtype or connexin36-deficient brain tissue (Figure 7E). The strongest expression of connexin36 was detected in the midbrain and hindbrain at postnatal day 10, while much weaker expression levels were found in the cerebellum, basal ganglia, hippocampus and cortex (Figure 7D). We used single molecule fluorescent in situ hybridization (using RNAscope) to define the neuronal cell types expressing *Bt-igsf* mRNAs, and in the midbrain observed co-expression with *vGlut1* and *GAD65*, indicating that *Bt-igsf* is expressed in both excitatory and inhibitory neurons (Figure 7F). Similar expression patterns were seen in the hippocampus (Extended Figure 2-2). Since the strongest expression of connexin36 was detected in the midbrain, we analyzed this region in more depth. No differences in the localization or expression of connexin36 protein were detected in the absence of BT-IgSF in

the midbrain and hindbrain (Figure 7G to K). We conclude that BT-IgSF modulates the expression of connexin43 specifically in astrocytes and ependymal cells, but does not affect localization or clustering of connexin36 in neurons.

Discussion

Here we show that the Ig cell adhesion molecule BT-IgSF (IgSF11/VSIG-3)) is highly expressed on astrocytes and ependymal cells of the mouse brain. Our functional analysis demonstrates that BT-IgSF is essential for the correct expression and subcellular localization of connexin43 in astrocytes and ependymal cells. In the absence of BT-IgSF, the level of connexin43 protein is severely reduced and fewer but larger clusters of connexin43 are formed on the surface of astrocytes and ependymal cells in the brain. Importantly, our analysis of gap junction coupling in BT-IgSF knockouts revealed a reduced astrocytic network in the cortex and hippocampus. However, this impaired coupling was not due to morphological changes of astrocytes in the absence of BT-IgSF. Astrocytes generate a complex syncytial network allowing them to interact with many neighboring cells to control a number of physiological processes like neurotransmission and disruptions of gap junction coupling are found in a broad spectrum of diseases such as neurodegeneration or epilepsy (Bedner and Steinhäuser, 2023; Huang et al., 2021; Mayorquin et al., 2018; Mazaud et al., 2021). A change in the localization pattern or expression level of connexin36 in neurons was not detected in the absence of BT-IgSF.

BT-IgSF is a member of a small and evolutionarily conserved subfamily of IgCAMs of which CAR was the founding member. This set of proteins mediates homotypic cell adhesion, share a common overall extracellular domain structure and a highly related amino acid sequence. A number of studies that relied on mouse mutants suggested that these proteins might undertake similar functions as they help to organize or regulate gap junctions in a variety of cell

types (Falk, 2020; Rathjen, 2020). For example, in the absence of CAR, connexin43 and 45 are reduced in the heart, resulting in impaired electrical conduction at the atrioventricular node (Lim et al., 2008; Lisewski et al., 2008; Pazirandeh et al., 2011). In addition, cultured embryonic CAR-deficient cardiomyocytes showed increased calcium cycling, increased beating frequency, altered connexin43 clustering and impaired dye coupling (Matthaeus et al., 2023). Another example is CLMP as the absence of this adhesion protein impaired the function in smooth muscle cells of the intestine and ureter. Accordingly, uncoordinated calcium signaling provoked a disturbed contraction of the intestine and ureter. Notably, the level of connexin43 and 45 proteins, but not their mRNAs, was severely reduced in the smooth muscle layers (Langhorst et al., 2018; Rathjen and Jüttner, 2023). Our studies on BT-IgSF described here provide an additional example of the way this subgroup of proteins plays a part in gap junction mediated cell-cell communication. The absence of BT-IgSF also affects the expression and localization pattern of connexin43 in astrocytes and ependymal cells. This is consistent with previously published data on the mis-localization of connexin43 in Sertoli cells of the testes, which leads to infertility and the functional impairment of the blood-testes-barrier (Pelz et al., 2017). Thus, all three members of the family, BT-IgSF, CLMP and CAR, are required for appropriate gap junction mediated cell-cell communication.

How might BT-IgSF exert its function on connexin43 in astrocytes?

Connexin43, much like other connexins, has a dynamic “life cycle” and possesses a half-life time of about 1-5 hours. Furthermore, connexins have a complex biosynthesis and can be degraded by multiple pathways. Many proteins are known to interact with connexins during all stages of the life cycle of a gap junction (Falk et al., 2016; Solan and Lampe, 2016). The reduced expression of connexin43 in BT-IgSF knockout astrocytes appears to be caused by increased degradation as revealed by our lysosomal pathway inhibition experiments and might

indicate a stabilization function of BT-IgSF on connexin43 at gap junctions. However, the intracellular localization of connexin43 to specific compartments was not altered, suggesting that intracellular trafficking of connexin43 might not be disturbed in the absence of BT-IgSF. The decreased amount of connexin43 might result in increased clustering at the cell surface and might therefore be a secondary effect. Interestingly, treatment of astrocyte cultures with tumor necrosis factor-α or interferon-γ caused a reduction of BT-IgSF that parallels the decrease of connexin43 by these factors. The latter finding was previously described on enterocytes of the intestine and on astrocytes (Hinkerohe et al., 2005; Leaphart et al., 2007; Meme et al., 2006; Zhang et al., 2015, 2013). Therefore, cytokines might be players that regulate the expression of BT-IgSF protein that in turn regulates connexin43 expression or localization. Reduced astrocyte-astrocyte coupling was also recently described in knockdown experiments of the Ig cell adhesion molecule HepaCAM (also termed GlialCAM) that, at the structural level is only distantly related to CAR subgroup members (Favre-Kontula et al., 2008; Moh et al., 2005). The authors found a reduced morphological complexity, including arborization of astrocytic protrusions, and a reduction in the territory covered by astrocytes. In addition, increased clustering of connexin43 was found in HepaCAM mutants and was accompanied by decreased dye coupling (Baldwin et al., 2021). Except for the increased clustering of connexin43 we did not detect similar morphological changes in astrocytes of BT-IgSF knockouts, nor did we find a reduction in astrocyte cell density in the molecular layer of the hippocampus. Moreover, HepaCAM is strongly expressed in the white matter, implicated in leukodystrophy and regulates the activity of glioblastoma cells (De et al., 2023; Favre-Kontula et al., 2008; Jeworutzki et al., 2012; López-Hernández et al., 2011) whereas the overall structure of the brain appears not to be affected by the absence of BT-IgSF (see Figures 1B, 1D, 6A, 2-1, 6-1). Therefore, HepaCAM and BT-IgSF seemingly play different roles, although in both cases their mutation resulted in impaired coupling. Furthermore, biochemical experiments established the direct association of HepaCAM with connexin43 at the cell surface (Baldwin et al., 2021; Wu

et al., 2016). By contrast, based on our co-localization studies in cultured astrocytes, we only occasionally detected BT-IgSF in close proximity with connexin43 at the cell surface of astrocytes, and we could not detect a direct interaction between the two proteins in co-precipitation experiments.

Co-localization of BT-IgSF with the scaffolding protein ZO-1 (Zona Occludens-1) at the cell surface was detected in Sertoli cells in confocal images (Pelz et al., 2017). BT-IgSF harbors a PDZ binding motif at its C-terminal domain and scaffolding proteins such as ZO-1 bind via a PDZ domain to most connexins (Hervé et al., 2014). Therefore, one might speculate that ZO-1 binds to BT-IgSF via its PDZ domain1, and to connexin43 via its PDZ domain 2 thus regulating connexin43 localization (Duffy et al., 2002). Furthermore, ZO-1 has been shown to control gap junction assembly as well as localization and influences plaque size in cell cultures (Hunter et al., 2005; Laing et al., 2005; Rhett et al., 2011). A frameshift mutation in the connexin43 gene in human patients suffering from oculo-dento digital dysplasia disrupts the connexin43-ZO-1 interaction (Bock et al., 2013; van Steensel et al., 2005). Despite these findings in other cell types, co-localization of ZO-1 with connexin43 or co-localization of BT-IgSF with connexin43 was only rarely detected at the plasma membrane of astrocytes. Nevertheless, a transient association of these components cannot be excluded. Additional studies with mice expressing mutant versions of BT-IgSF and ZO-1 to investigate possible interactions between BT-IgSF, ZO-1 and connexin43 might clarify whether these complexes play a role for connexin43 assembly or in stabilizing connexin43 at the plasma membrane of astrocytes. Currently the question of precisely how BT-IgSF controls connexin43 localization and expression needs to be investigated further. Additional studies are needed to thoroughly understand a possible signal transduction pathway downstream of BT-IgSF that modulates the de novo incorporation or removal of connexin43 to or from the plasma membrane.

BT-IgSF might have different functions in neurons and glial cells

Previously published knockdown studies using cultured hippocampal neurons from the CA1 region implicated BT-IgSF (IgSF11) in synaptic transmission through interactions with PSD95 and AMPA receptors (Jang et al., 2015). In these *in vitro* experiments, the BT-IgSF (IgSF11) knockdown caused increased mobility and endocytosis of AMPA receptors, suggesting that BT-IgSF is important for the stabilization of AMPA receptors in the neuronal plasma membrane. In accordance, BT-IgSF-deficient mice revealed a moderately decreased excitatory synaptic strength in the dentate gyrus and enhanced long-term potentiation in CA1 (Jang et al., 2015). Furthermore, BT-IgSF (IgSF11) was found to regulate the innervation of axons of chandelier cells on initial axon segments of pyramidal neurons (Hayano et al., 2021). To verify if our findings also apply to connexin localization in neurons, we extended our study and analyzed localization and expression of connexin36, the main neuronal connexin (Condorelli et al., 1998; Degen et al., 2004; Gulisano et al., 2000; Rubio and Nagy, 2015; Söhl et al., 1998). No differences in the localization or expression of connexin36 protein were detected in the absence of BT-IgSF in the midbrain. We conclude that BT-IgSF might have a different function in astrocytes and neurons, specifically modulating the expression of connexin43 in astrocytes and ependymal cells, but not affecting the distribution of connexin36 in neurons.

What might be the consequences of astrocyte network disturbance for neuronal function?

Astrocytes form an elaborate network to control a number of physiological processes in the brain. Disrupted communication of astrocytes in the absence of BT-IgSF could interfere with the coordination of astrocytic calcium waves or might affect synaptic activity. The close contact of astrocytic branches with synapses allows astrocytes to sense neuronal activity via their ion channels and neurotransmitter receptors (Ventura and Harris, 1999). Disruption of

astrocytic networks for example by inactivation of connexin43 and 30 reduced synaptic transmission (Charvériat et al., 2017; Giaume et al., 2010; Hardy et al., 2021; Pannasch et al., 2011; Perea et al., 2009; Pereda, 2014). Accordingly, connexin30 and astrocyte-targeted connexin43 knockout mice as well as connexin43 and 30 double knockout mice display impaired performance in sensorimotor and spatial memory tasks (Lutz et al., 2009; Theis et al., 2003). Astrocyte coupling is also altered in epilepsy (Bedner and Steinhäuser, 2023; Steinhäuser and Boison, 2012). Decreased coupling among astrocytes promotes neuronal hyperexcitability and attenuates seizure-induced histopathological outcomes (Deshpande et al., 2020). Astrocytic dysfunction is implicated in a number of neurodevelopmental disorders (Molofsk et al., 2012; Tan et al., 2021). Whether the behavioral deficits observed in BT-IgSF knockouts are caused by reduced astrocyte-astrocyte coupling or by deficits in the AMPA receptor trafficking needs further investigation using astrocyte- or neuron-specific ablation of BT-IgSF (Montag et al., 2023).

In the brain and spinal cord, ependymal cells line the ventricles and bear multiple cilia that beat in a concerted manner at their apical surface to drive cerebrospinal fluid circulation (Spassky and Meunier, 2017). This unidirectional movement might be coordinated by gap junction mediated cell-cell communication. Consistent with this hypothesis, *zebrafish* embryos injected with connexin43 morpholinos and connexin43-deficient mouse embryos exhibit a decreased number of cilia as well as diminished beating (Zhang et al., 2020).

In conclusion, in the present study we identified BT-IgSF as a crucial molecular helper to establish correct localization of connexin43 on astrocytes and ependymal cells. In astrocytes, this is essential for effective cell-cell coupling. Whether BT-IgSF's selective absence in astrocytes or ependymal cells is also important for neurotransmission or the coordinated movement of cilia, respectively, should be investigated in future work.

References

Ahi EP, Sefc KM (2017) A gene expression study of dorso-ventrally restricted pigment pattern in adult fins of Neolamprologus meeli, an African cichlid species. PeerJ 5:e2843.

Baldwin KT, Tan CX, Strader ST, Jiang C, Savage JT, Elorza-Vidal X, Contreras X, Rülicke T, Hippenmeyer S, Estévez R, Ji RR, Eroglu C (2021) HepaCAM controls astrocyte self-organization and coupling. Neuron 109:2427-2442.e10.

Bedner P, Steinhäuser C (2023) Role of Impaired Astrocyte Gap Junction Coupling in Epileptogenesis. Cells 12:1669.

Bock M de, Kerrebrouck M, Wang N, Leybaert L (2013) Neurological manifestations of oculodentodigital dysplasia: A Cx43 channelopathy of the central nervous system? Front Pharmacol 4 SEP:1–21.

Charvériat M, Naus CC, Leybaert L, Sáez JC (2017) Connexin-Dependent Neuroglial Networking as a New Therapeutic Target. Front Cell Neurosci 11:1–14.

Chen B, Zhu G, Yan A, He J, Liu Y, Li L, Yang X, Dong C, Kee K (2021) IGSF11 is required for pericentric heterochromatin dissociation during meiotic diplotene. PLoS Genet 17.

Condorelli DF, Parenti R, Spinella F, Salinaro AT, Belluardo N, Cardile V, Cicirata F (1998) Cloning of a new gap junction gene (Cx36) highly expressed in mammalian brain neurons. European Journal of Neuroscience 10:1202–1208.

De A, Lattier JM, Morales JE, Kelly JR, Zheng X, Chen Z, Sebastian S, Nassiri Toosi Z, Huse JT, Lang FF, McCarty JH (2023) Glial Cell Adhesion Molecule (GlialCAM) Determines Proliferative Versus Invasive Cell States in Glioblastoma. The Journal of Neuroscience JN-RM-1401-23.

Degen J, Meier C, van der Giessen RS, Söhl G, Petrasch-Parwez E, Urschel S, Dermietzel R, Schilling K, de Zeeuw CI, Willecke K (2004) Expression Pattern of lacZ Reporter Gene Representing Connexin36 in Transgenic Mice. Journal of Comparative Neurology 473:511–525.

Deng S, Gan L, Liu C, Xu T, Zhou S, Guo Y, Zhang Z, Yang GY, Tian H, Tang Y (2023) Roles of Ependymal Cells in the Physiology and Pathology of the Central Nervous System. Aging Dis.

Dermietzel R, Traub O, Hwang TK, Beyer E, Bennett M v, Spray DC, Willecke K (1989) Differential expression of three gap junction proteins in developing and mature brain tissues. Proc Natl Acad Sci U S A 86:10148–10152.

Deshpande T, Li T, Henning L, Wu Z, Müller J, Seifert G, Steinhäuser C, Bedner P (2020) Constitutive deletion of astrocytic connexins aggravates kainate-induced epilepsy. Glia 68:2136–2147.

Duffy HS, Delmar M, Spray DC (2002) Formation of the gap junction nexus: binding partners for connexins. Journal of Physiology-Paris 96:243–249.

Eom DS, Inoue S, Patterson LB, Gordon TN, Slingwine R, Kondo S, Watanabe M, Parichy DM (2012) Melanophore Migration and Survival during Zebrafish Adult Pigment Stripe Development Require the Immunoglobulin Superfamily Adhesion Molecule Igsf11. PLoSGenet 8:e1002899.

Falk MM (2020) Do CAR and CAR family members aid in gap junction formation? BioEssays 42:e2000276.

Falk MM, Bell CL, Kells Andrews RM, Murray SA (2016) Molecular mechanisms regulating formation, trafficking and processing of annular gap junctions. BMCCell Biol 17 Suppl 1:22–27.

Favre-Kontula L, Rolland A, Bernasconi L, Karmirantzou M, Power C, Antonsson B, Boschert U (2008) GlialCAM, an immunoglobulin-like cell adhesion molecule is expressed in glial cells of the central nervous system. Glia 56:633–645.

Giaume C, Koulakoff A, Roux L, Holcman D, Rouach N (2010) Astroglial networks: A step further in neuroglial and gliovascular interactions. Nat Rev Neurosci 11:87–99.

Güldenagel M, Ammermüller J, Feigenspan A, Teubner B, Degen J, Söhl G, Willecke K, Weiler R (2001) Visual transmission deficits in mice with targeted disruption of the gap junction gene connexin36. Journal of Neuroscience 21:6036–6044.

Gulisano M, Parenti R, Spinella F, Cicirata F (2000) Cx36 is dynamically expressed during early development of mouse brain and nervous system. Neuroreport 11:3823–3828.

Haffter P, Odenthal J, Mullins MC, Lin S, Farrell MJ, Vogelsang E, Haas F, Brand M, van Eeden FJ, Furutani-Seiki M, Granato M, Hammerschmidt M, Heisenberg CP, Jiang YJ, Kane DA, Kelsh RN, Hopkins N, Nusslein-Volhard C (1996) Mutations affecting pigmentation and shape of the adult zebrafish. Dev Genes Evol 206:260–276.

Harada H, Suzu S, Hayashi Y, Okada S (2005) BT-IgSF, a novel immunoglobulin superfamily protein, functions as a cell adhesion molecule. JCell Physiol 204:919–926.

Hardy E, Rancillac A, Cohen-salmon M, Rouach N (2021) Astroglial Cx30 differentially impacts synaptic activity from hippocampal principal cells and interneurons. Glia 69:2178–2198.

Hayano Y, Ishino Y, Hyun JH, Orozco CG, Steinecke A, Potts E, Oisi Y, Thomas CI, Guerrero-Given D, Kim E, Kwon H-B, Kamasawa N, Taniguchi H (2021) IgSF11 homophilic adhesion proteins promote layer-specific synaptic assembly of the cortical interneuron subtype. Sci Adv 7:1–14.

Hervé JC, Derangeon M, Sarrouilhe D, Bourmeyster N (2014) Influence of the scaffolding protein Zonula Occludens (ZOs) on membrane channels. Biochim Biophys Acta Biomembr 1838:595–604.

Higashine K, Hashimoto K, Tsujimoto E, Oishi Y, Hayashi Y, Miyamoto Y (2018) Promotion of differentiation in developing mouse cerebellar granule cells by a cell adhesion molecule BT-IgSF. Neurosci Lett 686:87–93.

Hinkerohe D, Smikalla D, Haghikia A, Heupel K, Haase CG, Dermietzel R, Faustmann PM (2005) Effects of cytokines on microglial phenotypes and astroglial coupling in an inflammatory coculture model. Glia 52:85–97.

Huang X, Su Y, Wang N, Li H, Li Z, Yin G, Chen H, Niu J, Yi C (2021) Astroglial Connexins in Neurodegenerative Diseases. Front Mol Neurosci 14:1–9.

Hunter AW, Barker RJ, Zhu C, Gourdie RG (2005) Zonula occludens-1 alters connexin43 gap junction size and organization by influencing channel accretion. Mol Biol Cell 16:5686–5698.

751 Irion U, Frohnhofer HG, Krauss J, Colak Champollion T, Maischein H-M, Geiger-Rudolph S, Weiler C,
752 Nusslein-Volhard C (2014) Gap junctions composed of connexins 41.8 and 39.4 are essential for
753 colour pattern formation in zebrafish. Elife 3:e05125.

754 Jang S et al. (2015) Synaptic adhesion molecule IgSF11 regulates synaptic transmission and plasticity.
755 Nat Neurosci 19:84–93.

756 Jeworutzki E, López-Hernández T, Capdevila-Nortes X, Sirisi S, Bengtsson L, Montolio M, Zifarelli G,
757 Arnedo T, Müller CS, Schulte U, Nunes V, Martínez A, Jentsch TJ, Gasull X, Pusch M, Estévez R
758 (2012) GlialCAM, a Protein Defective in a Leukodystrophy, Serves as a ClC-2 Cl - Channel
759 Auxiliary Subunit. Neuron 73:951–961.

760 Katoh MM, Katoh MM (2003) IGSF11 gene, frequently up-regulated in intestinal-type gastric cancer,
761 encodes adhesion molecule homologous to CXADR, FLJ22415 and ESAM. Int J Oncol 23:525–
762 531.

763 Kim GM, Kim J, Lee J-Y, Park M-C, Lee SY (2023) IgSF11 deficiency alleviates osteoarthritis in mice by
764 suppressing early subchondral bone changes. Exp Mol Med.

765 Kim H, Takegahara N, Choi Y (2023) IgSF11-mediated phosphorylation of pyruvate kinase M2
766 regulates osteoclast differentiation and prevents pathological bone loss. Bone Res 11:17.

767 Kim H, Takegahara N, Walsh MC, Middleton SA, Yu J, Shirakawa J, Ueda J, Fujihara Y, Ikawa M, Ishii
768 M, Kim J, Choi Y (2020) IgSF11 regulates osteoclast differentiation through association with the
769 scaffold protein PSD-95. Bone Res 8:5.

770 Laing JG, Chou BC, Steinberg TH (2005) ZO-1 alters the plasma membrane localization and function of
771 Cx43 in osteoblastic cells. J Cell Sci 118:2167–2176.

772 Laird DW, Lampe PD (2018) Therapeutic strategies targeting connexins. Nat Rev Drug Discov 17:905–
773 921.

774 Langhorst H, Jüttner R, Groneberg D, Mohtashamdolatshahi A, Pelz L, Purfürst B, Schmidt-Ott KM,
775 Friebe A, Rathjen FG (2018) The IgCAM CLMP regulates expression of Connexin43 and
776 Connexin45 in intestinal and ureteral smooth muscle contraction in mice. Dis Model Mech
777 11:dmm032128.

778 Leaphart CL, Qureshi F, Cetin S, Li J, Dubowski T, Batey C, Beer-Stolz D, Guo F, Murray SA, Hackam DJ
779 (2007) Interferon-γ Inhibits Intestinal Restitution by Preventing Gap Junction Communication
780 Between Enterocytes. Gastroenterology 132:2395–2411.

781 Li MWM, Mruk DD, Lee WM, Cheng CY (2010) Connexin 43 is critical to maintain the homeostasis of
782 the blood-testis barrier via its effects on tight junction reassembly. Proc Natl Acad Sci U S A
783 107:17998–18003.

784 Lim BK, Xiong D, Dorner A, Youn TJ, Yung A, Liu TI, Gu Y, Dalton ND, Wright AT, Evans SM, Chen J,
785 Peterson KL, McCulloch AD, Yajima T, Knowlton KU (2008) Coxsackievirus and adenovirus
786 receptor (CAR) mediates atrioventricular-node function and connexin 45 localization in the
787 murine heart. JClinInvest 118:2758–2770.

788 Lisewski U, Shi Y, Wrackmeyer U, Fischer R, Chen C, Schirdewan A, Jüttner R, Rathjen F, Poller W,
789 Radke MHMH, Gotthardt M (2008) The tight junction protein CAR regulates cardiac conduction
790 and cell-cell communication. J Exp Med 205:2369–2379.

López-Hernández T, Ridder MC, Montolio M, Capdevila-Nortes X, Polder E, Sirisi S, Duarri A, Schulte U, Fakler B, Nunes V, Scheper GC, Martínez A, Estévez R, Van Der Knaap MS (2011) Mutant GlialCAM causes megalencephalic leukoencephalopathy with subcortical cysts, benign familial macrocephaly, and macrocephaly with retardation and autism. Am J Hum Genet 88:422–432.

Lutz SE, Zhao Y, Gulinello M, Lee SC, Raine CS, Brosnan CF (2009) Deletion of astrocyte connexins 43 and 30 leads to a dysmyelinating phenotype and hippocampal CA1 vacuolation. Journal of Neuroscience 29:7743–7752.

Maglione M, Tress O, Haas B, Karram K, Trotter J, Willecke K, Kettenmann H, Trotter J, Maglione M, Karram K, Tress O, Haas B, Kettenmann H (2010) Oligodendrocytes in mouse corpus callosum are coupled via gap junction channels formed by connexin47 and connexin32. Glia 58:1104–1117.

Matthaeus C, Jüttner R, Gotthardt M, Rathjen FG (2022) The IgCAM CAR Regulates Gap Junction-Mediated Coupling on Embryonic Cardiomyocytes and Affects Their Beating Frequency. Life 13:14.

Mayorquin LC, Rodriguez A v., Sutachan JJ, Albarracín SL (2018) Connexin-mediated functional and metabolic coupling between astrocytes and neurons. Front Mol Neurosci 11:1–10.

Mazaud D, Capano A, Rouach N (2021) The many ways astroglial connexins regulate neurotransmission and behavior. Glia 69:2527–2545.

McCarthy K, de Vellis J (1980) Preparation of separate astroglial and oligodendroglial cell cultures from rat cerebral tissue. JCell Biol 85:890–902.

Meme W, Calvo C, Froger N, Ezan P, Amigou E, Koulakoff A, Giaume C (2006) Proinflammatory cytokines released from microglia inhibit gap junctions in astrocytes: potentiation by β-amyloid. The FASEB Journal 20:494–496.

Moh MC, Zhang C, Luo C, Lee LH, Shen S (2005) Structural and functional analyses of a novel Ig-like cell adhesion molecule, hepaCAM, in the human breast carcinoma MCF7 cells. Journal of Biological Chemistry 280:27366–27374.

Molofsk A v., Krenick R, Ullian E, Tsai HH, Deneen B, Richardson WD, Barres BA, Rowitch DH (2012) Astrocytes and disease: A neurodevelopmental perspective. Genes Dev 26:891–907.

Montag D, Pelz L, Rathjen FG (2023) Lack of the Ig cell adhesion molecule BT-IgSF (IgSF11) induced behavioral changes in the open maze, water maze and resident intruder test. PLoS One 18:4–15.

Musil LS, Goodenough DA (1991) Biochemical analysis of connexin43 intracellular transport, phosphorylation, and assembly into gap junctional plaques. Journal of Cell Biology 115:1357–1374.

Nagy JI, Dudek FE, Rash JE (2004) Update on connexins and gap junctions in neurons and glia in the mammalian nervous system. Brain Res Rev 47:191–215.

Owczarek C, Elmasry Y, Parsons M (2023) Contributions of coxsackievirus adenovirus receptor to tumorigenesis. Biochem Soc Trans 51:1143–1155.

Pannasch U, Vargova L, Reingruber J, Ezan P, Holcman D, Giaume C, Sykova E, Rouach N (2011) Astroglial networks scale synaptic activity and plasticity. Proceedings of the National Academy of Sciences 108:8467–8472.

Pazirandeh A et al. (2011) Multiple phenotypes in adult mice following inactivation of the Coxsackievirus and Adenovirus Receptor (Car) gene. PLoS One 6:e20203.

Pelz L, Purfürst B, Rathjen FG (2017) The cell adhesion molecule BT-IgSF is essential for a functional blood-testis barrier and male fertility in mice. Journal of Biological Chemistry 292:21490–21503.

Perea G, Navarrete M, Araque A (2009) Tripartite synapses: astrocytes process and control synaptic information. Trends Neurosci 32:421–431.

Pereda AE (2014) Electrical synapses and their functional interactions with chemical synapses. Nat Rev Neurosci 15:250–263.

Raschperger E, Engstrom U, Pettersson RF, Fuxe J (2004) CLMP, a novel member of the CTX family and a new component of epithelial tight junctions. Journal of Biological Chemistry 279:796–804.

Rathjen FG (2020) The CAR group of Ig cell adhesion proteins – Regulators of gap junctions ? BioEssays 42:1–11.

Rathjen FG, Jüttner R (2023) The IgSF Cell Adhesion Protein CLMP and Congenital Short Bowel Syndrome (CSBS). Int J Mol Sci 24:5719.

Rhett JM, Jourdan J, Gourdie RG (2011) Connexin 43 connexon to gap junction transition is regulated by zonula occludens-1. Mol Biol Cell 22:1516–1528.

Richter N, Wendt S, Georgieva PB, Hambardzumyan D, Nolte C, Kettenmann H (2014) Glioma-associated microglia and macrophages/monocytes display distinct electrophysiological properties and do not communicate via gap junctions. Neurosci Lett 583:130–135.

Roessmann U, Velasco ME, Sindely SD, Gambetti P (1980) GLIAL FIBRILLARY ACIDIC PROTEIN (GFAP) IN EPENDYMAL CELLS DURING DEVELOPMENT. AN IMMUNOCYTOCHEMICAL STUDY, Brain Research.

Rubio ME, Nagy JI (2015) Connexin36 expression in major centers of the auditory system in the CNS of mouse and rat: Evidence for neurons forming purely electrical synapses and morphologically mixed synapses. Neuroscience 303:604–629.

Saunders NR, Dziegielewska KM, Møllgård K, Habgood MD (2018) Physiology and molecular biology of barrier mechanisms in the fetal and neonatal brain. J Physiol 596:5723–5756.

Schrezenmeier E, Dörner T (2020) Mechanisms of action of hydroxychloroquine and chloroquine: implications for rheumatology. Nat Rev Rheumatol.

Singh AP, Nusslein-Volhard C (2015) Zebrafish stripes as a model for vertebrate colour pattern formation. Curr Biol 25:R81–R92.

Söhl G, Degen J, Teubner B, Willecke K (1998) The murine gap junction gene connexin36 is highly expressed in mouse retina and regulated during brain development. FEBS Lett 428:27–31.

Solan JL, Lampe PD (2016) Kinase programs spatiotemporally regulate gap junction assembly and disassembly: Effects on wound repair. SeminCell DevBiol 50:40–48.

Spassky N, Meunier A (2017) The development and functions of multiciliated epithelia. Nat Rev Mol Cell Biol 18:423–436.

Steinhäuser C, Boison D (2012) Epilepsy: Crucial role for astrocytes. Glia 60:1191.

870 Suzu S, Hayashi Y, Harumi T, Nomaguchi K, Yamada M, Hayasawa H, Motoyoshi K (2002) Molecular
871 cloning of a novel immunoglobulin superfamily gene preferentially expressed by brain and
872 testis. BiochemBiophysResCommun 296:1215–1221.

873 Tan CX, Burrus Lane CJ, Eroglu C (2021) Role of astrocytes in synapse formation and maturation. Curr
874 Top Dev Biol 142:371–407.

875 Theis M, Jauch R, Zhuo L, Speidel D, Wallraff A, Döring B, Frisch C, Söhl G, Teubner B, Euwens C,
876 Huston J, Steinhäuser C, Messing A, Heinemann U, Willecke K (2003) Accelerated hippocampal
877 spreading depression and enhanced locomotory activity in mice with astrocyte-directed
878 inactivation of connexin43. Journal of Neuroscience 23:766–776.

879 van Steensel MAM, Spruijt L, van der Burgt I, Bladergroen RS, Vermeer M, Steijlen PM, van Geel M
880 (2005) A 2-bp deletion in the GJA1 gene is associated with oculo-dento-digital dysplasia with
881 palmoplantar keratoderma. Am J Med Genet A 132A:171–174.

882 Ventura R, Harris KM (1999) Three-dimensional relationships between hippocampal synapses and
883 astrocytes. Journal of Neuroscience 19:6897–6906.

884 Wang F, Flanagan J, Su N, Wang LC, Bui S, Nielson A, Wu X, Vo HT, Ma XJ, Luo Y (2012) RNAscope: A
885 novel in situ RNA analysis platform for formalin-fixed, paraffin-embedded tissues. Journal of
886 Molecular Diagnostics 14:22–29.

887 Wang J et al. (2019) VSIG-3 as a ligand of VISTA inhibits human T-cell function. Immunology 156:74–
888 85.

889 Watanabe M, Iwashita M, Ishii M, Kurachi Y, Kawakami A, Kondo S, Okada N (2006) Spot pattern of
890 leopard Danio is caused by mutation in the zebrafish connexin41.8 gene. EMBO Rep 7:893–897.

891 Watanabe M, Kondo S (2012) Changing clothes easily: connexin41.8 regulates skin pattern variation.
892 Pigment Cell Melanoma Res 25:326–330.

893 Willecke K, Eiberger J, Degen J, Eckardt D, Romualdi A, Guldenagel M, Deutsch U, Sohl G (2002)
894 Structural and functional diversity of connexin genes in the mouse and human genome.
895 BiolChem 383:725–737.

896 Wu M, Moh MC, Schwarz H (2016) HepaCAM associates with connexin 43 and enhances its
897 localization in cellular junctions. Sci Rep 6:36218.

898 Xie X, Chen C, Chen W, Jiang J, Wang L, Li T, Sun H, Liu J (2021) Structural Basis of VSIG3: The Ligand
899 for VISTA. Front Immunol 12.

900 Zhang FF, Morioka N, Kitamura T, Hisaoka-Nakashima K, Nakata Y (2015) Proinflammatory cytokines
901 downregulate connexin 43-gap junctions via the ubiquitin-proteasome system in rat spinal
902 astrocytes. Biochem Biophys Res Commun 464:1202–1208.

903 Zhang FF, Morioka N, Nakashima-Hisaoka K, Nakata Y (2013) Spinal astrocytes stimulated by tumor
904 necrosis factor-α and/or interferon-γ attenuate connexin 43-gap junction via c-jun terminal
905 kinase activity. J Neurosci Res 91:745–756.

906 Zhang J et al. (2020) Wnt-PLC-IP3-Connexin-Ca2+ axis maintains ependymal motile cilia in zebrafish
907 spinal cord. Nat Commun 11:1860.

908

Figure Legends

Figure 1

Impaired clustering of connexin43 in astrocytes in the absence of BT-IgSF.

A and B) Overview of the location of connexin43 in coronal sections of the hippocampus from wildtype (A) and BT-IgSF-deficient (B) mice (10 weeks old). CA1, cornus ammonis 1; CA3, Cornus ammonis 3; DG, dendate gyrus; GCL, granule cell layer; ML, molecular layer. Scale bar, 100 µm.

C) Higher magnification of the molecular layer of the dentate gyrus from adult wildtype and knockout mice stained by mAb anti-connexin43, rabbit anti-BT-IgSF and DAPI. Arrow heads indicate large connexin43 clusters.

D) Cortical astrocyte monolayer cultures from P3 wildtype or knockout mice at DIV14 stained by mAb anti-connexin43, rabbit anti-BT-IgSF and DAPI. Scale bar, 20µm.

E and F) Quantification of the connexin43 spots and cluster size on astrocytes in the hippocampus. In total 1652.5±306.6 (mean ± SD) and 505.4±128.1 (mean ± SD) connexin43 spots from wildtype and BT-IgSF -/-, respectively, from 10 cryo-sections (63x objective) of three specimens of each genotype were counted. Nested t-test was applied.

H and I) Quantification of the connexin43 spots and cluster size of connexin43 on cultured cortical astrocytes. Control, 243±65.1 (mean ± SD); BT-IgSF-/-, 132.9±43.9 spots from 10 view fields (100x objective) from three independent cultures per genotype were counted. Nested t-test.

G and J) Cluster size distribution of connexin43 versus cluster number in the hippocampus or on astrocytes in culture (J).

Scale bar in B, 100 µm; in C and D, 20µm.

Figure 2

Expression of BT-IgSF on astrocytes (see Figure 2-1 for BT-IgSF antibody specificity and Figure 2-2 for BT-IgSF mRNA expression in neurons).

A) Localization of BT-IgSF in hippocampus cells from P2-old mice cultured for 10 days *in vitro* and stained by guinea pig antibodies to GFAP and rabbit anti-BT-IgSF. Three independent cultures were analyzed. Scale bar, 20 µm.

B) Western blot of extracts from an astrocyte culture using rabbit antibodies to BT-IgSF. Extracts from two cultures were mixed and three times analyzed by blots. Molecular mass markers are indicated at the left of the panel.

C) Cultured hippocampus cells were stained by antibodies to MAP2a/b and rabbit anti-BT-IgSF. Three cultures were analyzed. Scale bar, 30 µm. BT-IgSF is found on GFAP astrocytes but rarely detectable on MAP2a/b-positive neurons by antibodies.

D) Localization of BT-IgSF in a coronal hippocampus section from an adult mouse. BT-IgSF is primarily found in the molecular layer and the subgranular zone. Higher magnification shows a widespread localization in the molecular layer probably not restricted to a specific cell type. Five independent experiments were done. CA1, cornus ammonis 1; CA3, Cornus ammonis 3; DG, dendate gyrus; GCL, granule cell layer; ML, molecular layer. Left and middle panel, scale bar 1 mm; right panel 20 µm.

E) RNAscope of a coronal section of the hippocampus at P20 showing expression of *Bt-igsf* mRNA in GFAP-positive astrocytes in the molecular layer and hilus of the dentate gyrus. Three independent sections were analyzed. Scale bar, 50 µm.

F) Higher magnifications of squares as indicated in E). Scale bar, 5 µm.

G) Effective extraction of BT-IgSF from tissues requires SDS. Equal amounts of crude membrane fractions from brain (P56) were extracted with 1% TX100 or SDS. For specificity of the antibody knockout brain tissue is shown. Three independent extractions were done.

960 H and I) Different postnatal stages of brain extracts using SDS stained with anti-BT-IgSF are
961 shown (n=3). BT-IgSF is primarily found at advanced postnatal stages. Anti-GAPDH indicates
962 loading. J) For comparison GFAP expression is shown.
963
964
965 **Figure 3**
966 **Connexin43 but not connexin30 proteins are reduced in the hippocampus and cortex, and**
967 **blockers of the protein biosynthesis and proteolysis show increased degradation of**
968 **connexin43 in the absence of BT-IgSF.**
969 A, B and C) Western blots demonstrating reduction of connexin43 in crude membrane
970 fractions from 8 weeks-old hippocampi or cortices of wildtype and BT-IgSF-deficient mice.
971 The crude membrane fractions were first solubilized in 1% Triton-X100 and un-solubilized
972 material was then solved in 1% SDS. 20 µg of protein was loaded per lane. Loading control is
973 demonstrated by a monoclonal antibody to the heavy chain of clathrin. Quantification of band
974 intensities are shown in B. For hippocampus 5 and 6 specimen for each genotype were
975 analyzed for TX-100 and SDS, respectively; for cortex 7 and 7 for TX-100 and SDS,
976 respectively. In Figure 3C for each condition 3 specimens were inspected.
977 Blot intensities of the BT-IgSF mutant were normalized to control (CON) values. p-values
978 above the columns indicate significance to controls. Mann-Whitney-test.
979 For comparison quantification of Western blots of antibodies to connexin30 are shown in C.
980 D) The localization of connexin30 in the molecular layer of hippocampi is not affected by the
981 absence of BT-IgSF. DG, dentate gyrus; ML, molecular layer. Scale bar, 20 µm.
982 E and F) The expression of GFAP is not reduced in the absence of BT-IgSF. Equal loading is
983 indicated by an antibody to GAPDH. For each condition 4 specimens were analyzed.
984 G and H) Astrocytes treated with cycloheximide (100 µg/ml) for times indicated in the
985 Figures were lysed (1% SDS in TBS and 1 mM EDTA supplemented with protease blockers)

and boiled in SDS sample buffer. Equal amounts were loaded on 10 % SDS PAGE, blotted and analyzed with rabbit anti-connexin43. Equal loading was controlled by mAb to GAPDH. Quantification of all cycloheximide experiments was done using Image Lab software (BioRad). At each condition multiple cultures from 4 mice of each genotype were run on multiple Western blots (7 to 24). No significance was measured between genotypes; nested t-test and an outlier test were applied.

I and J) Blocking of lysosomal degradation by chloroquine (CQ) (100 µM) for 4 hours in astrocyte cultures from control and BT-IgSF knockouts. At each condition multiple cultures from 3 mice of each genotype were run on multiple Western blots (16 to 20). Outlier-test and nested t-test were applied, in addition for 3J knockout data were analyzed by Mann-Whitney of the means of the blot replicates for each independent culture (p=0.0286).

Figure 4

Subcellular localization of connexin43 is not impaired in the absence of BT-IgSF

A – D) The subcellular localization of connexin43 in the absence of BT-IgSF and wildtype astrocytes was analyzed by using phalloidin or specific antibodies to intracellular subcellular compartments. Cells from three independent cultures were fixed with 4% paraformaldehyde/PBS (5 minutes on ice) before application of the antibodies and analyzed as described in the Materials and Method section.

A) mAb to γ-adaptin and rabbit anti-connexin43,

B) mAb to GM130 and rabbit anti-connexin43,

C) mAb to LAMP-1 and rabbit anti-connexin43,

D) phalloidin-594 and rabbit anti-connexin43.

E) Cell surface localization of connexin43 clusters on BT-IgSF-deficient astrocytes in culture. Living cells were incubated with WGA-488 for 45 minutes on ice, then fixed and

permeabilized followed by staining with rabbit anti-connexin43. Connexin43 (Red) spots were counted on BT-IgSF -/- astrocytes from three independent cultures (100x objective). Strong co-localization was observed between WGA-488 (Green) and connexin43. Numbers are as follows: Experiment 1: 470 connexin43-positive spots (95%) showed co-localization with WGA, 29 not (10 cells analyzed). Experiment 2: 329 (98%) versus 3 (5 cells). Experiment 3: 519 (98%) versus 14 (7 cells).

F) mAb to ZO-1 and rabbit anti-connexin43,

G) Rb96 to BT-IgSF and mAb to connexin43. Mean values and standard deviations of the three independent cultures are: – 0.02037 (SD 0.2666), 0.07 (SD 0.2768) and -0.0063 (SD 0.2334). The ONE-ANOVA value of 0.1632 indicates similarity between the three cultures. In A to D and F) n=27-30, in G n=82 images were analyzed for the calculation of the Pearson's R value. The number of experimental replicates for 4A to G was 3. Nested t-test was applied. Scale bar in A-D and F and G, 10 µm; scale bar in E, 5 µm.

H – J) Expression of BT-IgSF protein is decreased in the presence of tumor necrosis factor-α (1 ng/ml) or interferon-γ (10 ng/ml) on astrocytes in culture (H and I). Both reagents were applied for 24 hr in DMEM without FCS. Four independent wildtype cultures were analyzed in multiple Western blots (IFN-γ: 14 and 15; TNF-α: 9 and 10). For comparison reduced expression of connexin43 in the presence of tumor necrosis factor-α or interferon-γ is shown (J). Gels using antibodies to BT-IgSF were run under non-reducing conditions. Nested t-tests were applied and additionally Mann-Whitney test for IFN-γ or of TNF-α treatments of the means of biological replicates were performed (p=0.0280 and p=0.0286, respectively).

Figure 5

Impaired gap junction mediated coupling between astrocyte networks in the BT-IgSF knockout mice (see Figure 5-1 for electrophysiological data).

A) Scheme of homophilic binding of BT-IgSF, B) connexin43 coupling and C) the dye filling experiment to study gap junctional communication in astrocytes. PM – plasma membrane.

D) z-stack images of both genotypes of the immunohistochemical analysis for DAPI, biocytin, BT-IgSF and GFAP staining in hippocampus. The right images show an overlay of all channels. GCL, granular cell layer; ML, molecular layer. Scale bar, 100 µm.

E - G) Scatter plots showing the network size (E, number of coupled cells), tracer spread alongside (F, tracer-spread x) or perpendicular to the Schaffer collaterals (G, tracer-spread y). 15 dye-filled slices from 3 control mice and 11 slices from 4 BT-IgSF knockout mice were analyzed. On average 101±8.851 (mean ± SD) biocytin-positive hippocampal astrocytes were coupled in the wildtype, whereas in the knockout only 78±7.837 (mean ± SD) biocytin-positive astrocytes were found to form a network. Nested t-test.

H - J) Scatter blots of dye-coupling of astrocytes in the cortex. On average 118±20.95 (mean ± SD) astrocytes in control and 48±7.86 (mean ± SD) in the BT-IgSF knockout form a network (11 dye-filled slices from 4 controls and 10 slices from 4 knockouts). Nested t-test.

K) Area of individual cultured astrocytes is not affected by the absence of BT-IgSF (3 independent cultures of each genotype). Nested t-test.

L) Number of GFAP-positive astrocytes is not reduced in the absence of BT-IgSF. GFAP-positive cells were counted in microscopic view fields (350 µm x 350 µm) in the molecular layer of sections of hippocampi from wildtype and BT-IgSF knockout mice. 964 cells in 15 view fields and 616 cells in 9 view fields were counted for wildtype and knockout, respectively. Numbers of replicates were 4 for the control and 3 for the BT-IgSF knockout. Nested t-test and in addition Mann-Whitney of the means of the replicates (p=0.700).

M) Images of GFAP-positive astrocytes in the molecular layer of the hippocampus from wildtype and BT-IgSF-deficient mice indicating a similar morphology.

N) Branching of GFAP-positive cells remains unchanged in the absence of BT-IgSF. Primary GFAP-positive branches were counted in the molecular layer of the hippocampus. 46 and 41

cells were analyzed for wildtype and knockout, respectively. Numbers of replicates were 4 for the control and 3 for the BT-IgSF knockout. Nested t-test.

Figure 6

Expression of BT-IgSF on ependymal cells and impaired localization of connexin43 on ependymal cells in the absence of BT-IgSF (see Figure 6-1 for BT-IgSF antibody specificity on ependymal cells).

A) Expression of BT-IgSF in ependymal cells of the lateral, third ventricle and central canal by immunohistochemistry using an antibody to the extracellular domain of BT-IgSF. E15 lateral ventricle, scale bar 400 µm; P7 third ventricle, 50 µm; central canal of an E12.5 spinal cord, transversal section; dorsal is up, scale bar 100 µm. Red, anti-BT-IgSF; blue, DAPI. For specificity of the antibody sections of BT-IgSF knockout tissue are shown.

B) Higher magnification of the ependymal cell layer showing expression of BT-IgSF at lateral and basal sides of ependymal cells in the lateral ventricle of an adult wildtype mouse. Co-localization of BT-IgSF and GFAP in the ependyma is shown. Ventricle and the apical side of the ependymal cells (indicated by arrow heads) are at the bottom of the image. Scale bar, 20 µm.

C) BT-IgSF is not or only weakly found at the choroid plexus in contrast to the related CAR. Coronal sections from regions of the lateral ventricle from a 19-week-old mouse were stained with rabbit antibodies to BT-IgSF (Rb95) or to CAR (Rb80) and DAPI.

D) Clustering of connexin43 on ependymal cells of the lateral ventricle from adult wildtype and BT-IgSF knockout mice. Ventricle is at the top of the images. Arrow heads indicate large connexin43 cluster. Scale bar, 20 µm.

E - G) Quantification of the number of connexin43 spots, size and distribution of number versus size as described for astrocytes. Control, 283.5±58.8; BT-IgSF-/-, 132.9±145.8 (mean ± SD) spots from 10 view fields (63x objective) from three animals per genotype. Nested t-test.

Figure 7

Connexin36 localization on neurons is not impaired in the absence of BT-IgSF

A - D) Specificity of antibodies to connexin36 in Western blots using crude membrane fractions from wildtype and connexin36-deficient P10 brain tissues. 12 µg of protein was loaded per lane. In A) mAb to connexin36 (sc-398063), in B) mAb to connexin36 (8F6.2), in C) rabbit to connexin36 (364600) and in D) rabbit antibody to connexin36 generated in this study (amino acid residues 99 to 197) are shown. Satisfactory specificity could only be demonstrated for antibody shown in D). A 34 kD protein (arrow heads) was specifically detected in wildtype but not in connexin36-deficient tissues. However, a prominent unspecific band at 52 kD was detected in both genotypes.

E) Specificity of rabbit antibody to connexin36 (residues 99 to 197) in sagittal sections of P10 superior colliculus from wildtype and connexin36-deficient mice. Nf, neurofilament.

F) RNAscope demonstrating neuronal expression of BT-IgSF in sagittal sections from P10 superior colliculus.

G to H) Localization and clustering of connexin36 is not altered in P10 sagittal sections of the midbrain in the absence of BT-IgSF. Scale bar, 20µm. Nf, neurofilament. The number of connexin36 spots in the midbrain were counted in 3 cryo-sections of 4 animals of each genotype. In both cases 2500 μm^2 were analyzed by image J software for each section. Nested t-test.

I to K) Connexin36 protein is not altered in the absence of BT-IgSF. Hindbrain (I) and midbrain (J), control n=3; knockout, n=4. Mann-Whitney test.

Table 1: Antibodies for immunohistochemistry, immunocytochemistry and for Western blotting

Antibody	IHC and ICC	Western blots	Source
mAb γ-adaptin RRID:AB_397768	1 µg/ml		BD Transduction Laboratories #610385
Rabbit anti-mBT-IgSF-Fc (Rb95 or Rb96) IgG	1-3 µg/ml	1 µg/ml	Pelz et al., 2017
Rabbit anti-mCAR	1 µg/ml		Patzke et al., 2010
mAb anti-connexin43 RRID:AB_397473	1 µg/ml		BD Transduction Laboratories, #610061
Rabbit anti-connexin43 RRID:AB_2294590	1:200	1:1000	Cell signaling, #3512
Rabbit anti-connexin30 RRID:AB_2533979	1 µg/ml	0.5 µg/ml	Invitrogen #71-2200
Rabbit anti-connexin36 RRID:AB_2533260		1 µg/ml	Zymed/Invitrogen 36-4600
mAb connexin36 (H9)		1 µg/ml	Santa Cruz sc-398063
Rabbit anti-m-connexin36 (RbB5)	0.5 µg/ml	0.5 µg/ml	This study
mAb 2H3 anti-neurofilament RRID:AB_531793	7.5 µg/ml		mAb 2H3 Developmental Hybridoma Bank
mAb 8F6.2 connexin35/36 RRID:AB_94632		1 µg/ml	Millipore MAB3045
mAb ZO-1 RRID:AB_2533147	1:200		Invitrogen #339100
Guinea pig anti-GFAP RRID:AB_10641162	1:500	1:1000	Synaptic Systems#173004
Goat anti-GFAP RID:AB_641021	1:200	1:1000	Santa Cruz #sc-6170
Rabbit anti-GFAP RRID:AB_10013382	1:1000		Dako Z0334
mAb GM130 RRID:AB_398142	1 µg/ml		BD Transduction Laboratories # 610823
mAb LAMP-1 (1D4B)	1 µg/ml		Santa Cruz ,sc-19992

RRID:AB_2134495			
mAb anti-MAP2a/b (clone AP20)	1:500	1:1000	Dianova#DLN-08578
Rabbit anti-ZO-1 RRID:AB_2533456	1:100		Invitrogen #40-2200
mAb anti-GAPDH (1D4) RRID:AB_10077627		0.5 µg/ml	Novus Biologicals, #NB300-221
mAb anti-Clathrin (heavy chain) RRID:AB_397865		1:1000	BD Transduction Laboratories #610499
Goat anti-Rabbit-Cy3	1:400 – 1:1000		Dianova
Goat anti-Mouse-Alexa488	1:400 – 1:1000		Molecular Probes
Rabbit anti-Goat-Alexa488	1:500 – 1:1000		Dianova
Goat anti-Rabbit-HRP		1:20 000	Dianova
Goat anti-Mouse-HRP		1:20 000	Dianova

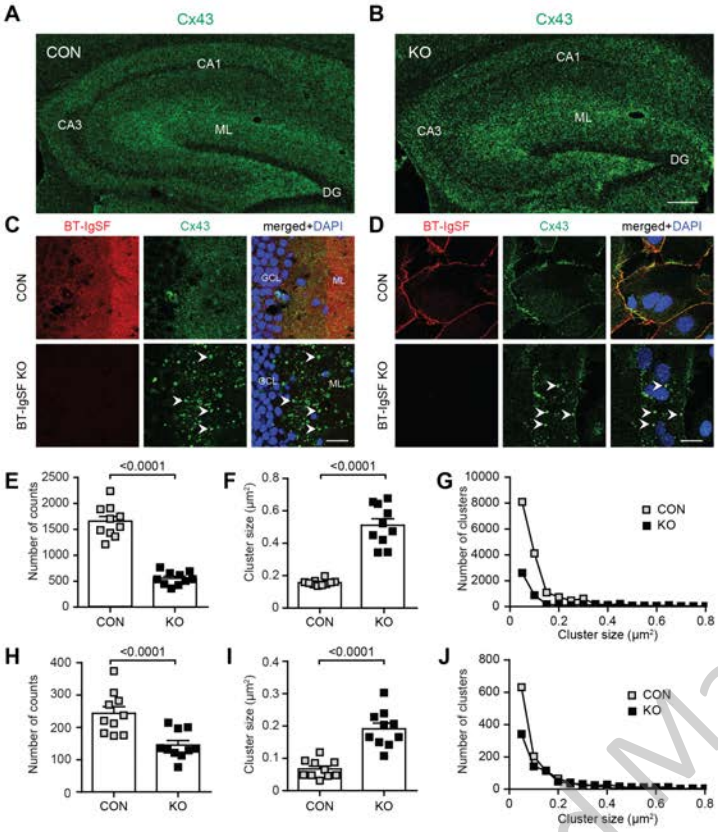

Figure 1

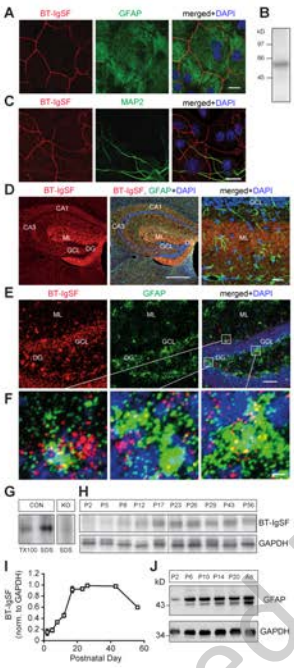

Figure 2

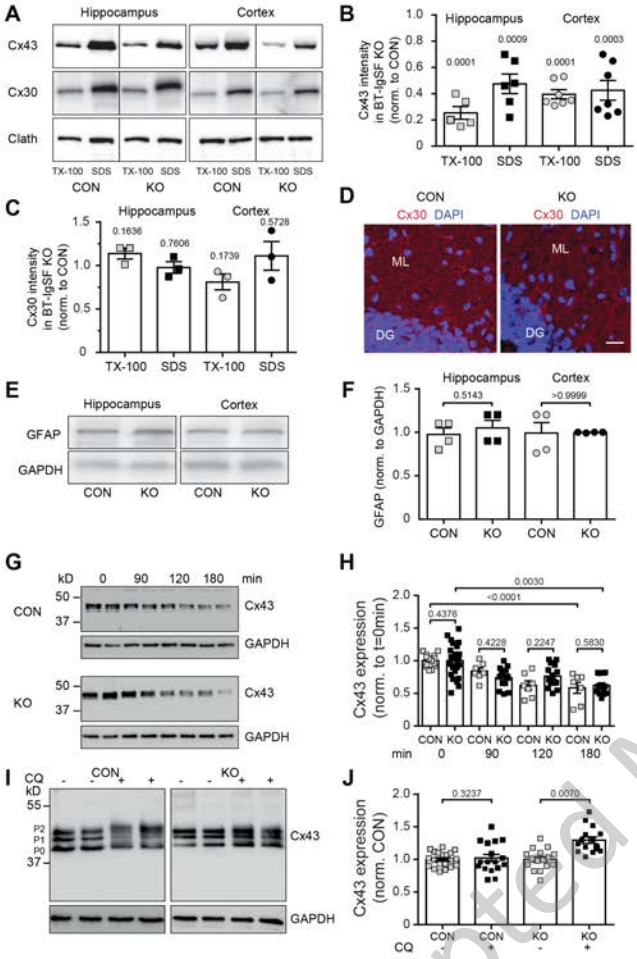

Figure 3

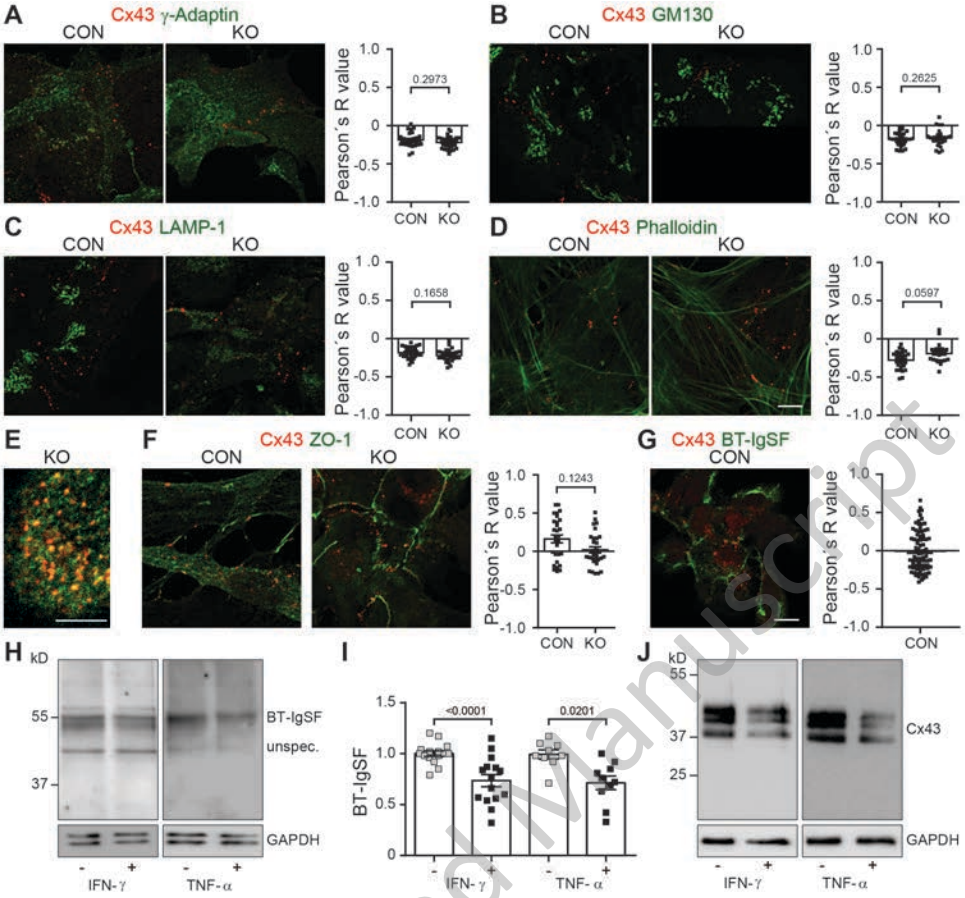

Figure 4

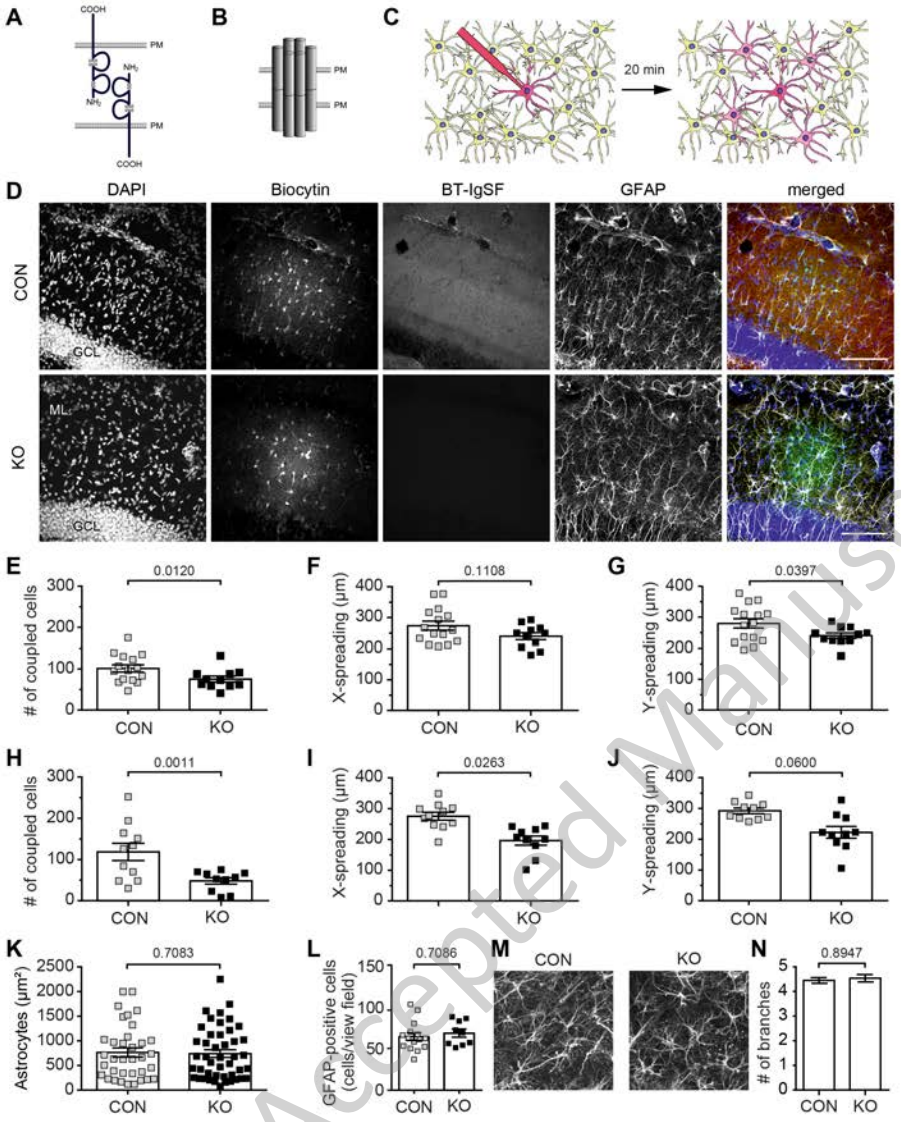

Figure 5

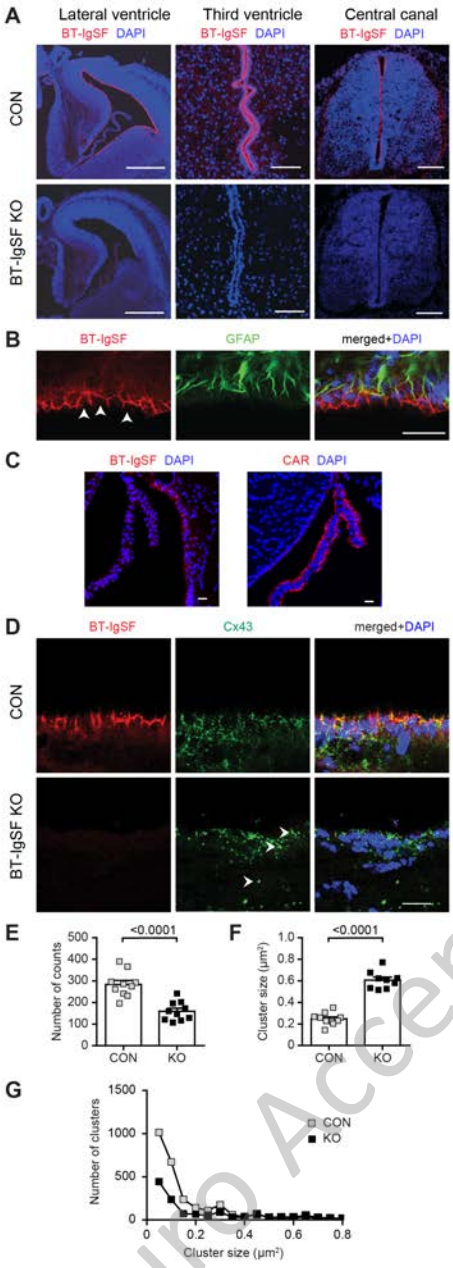

Figure 6

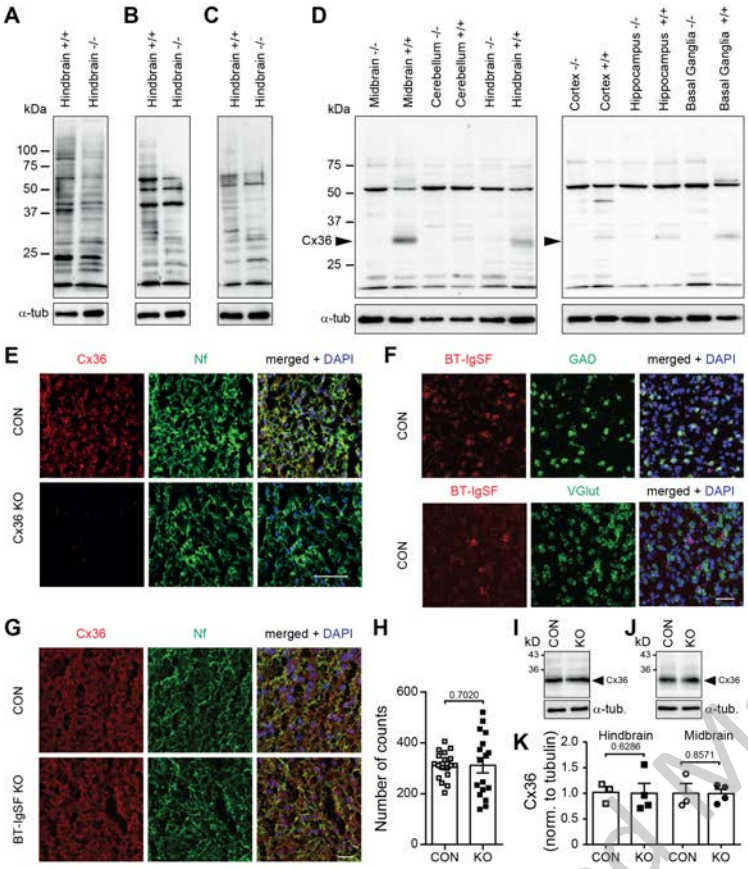

Figure 7